

# Stau as the Lightest Supersymmetric Particle in $R$ -Parity Violating SUSY Models: Discovery Potential with Early LHC Data

K. Desch,<sup>\*</sup> S. Fleischmann,<sup>†</sup> and P. Wienemann<sup>‡</sup>  
*Physics Institute, University of Bonn, Bonn, Germany*

H. K. Dreiner<sup>§</sup>

*Bethe Center for Theoretical Physics and Physics Institute, University of Bonn, Bonn, Germany and  
 SCIPP, University of California, Santa Cruz, CA 95064, USA*

S. Grab<sup>¶</sup>

*SCIPP, University of California, Santa Cruz, CA 95064, USA*

We investigate the discovery potential of the LHC experiments for  $R$ -parity violating supersymmetric models with a stau as the lightest supersymmetric particle (LSP) in the framework of minimal supergravity. We classify the final states according to their phenomenology for different  $R$ -parity violating decays of the LSP. We then develop event selection cuts for a specific benchmark scenario with promising signatures for the first beyond the Standard Model discoveries at the LHC. For the first time in this model, we perform a detailed signal over background analysis. We use fast detector simulations to estimate the discovery significance taking the most important Standard Model backgrounds into account. Assuming an integrated luminosity of  $1 \text{ fb}^{-1}$  at a center-of-mass energy of  $\sqrt{s} = 7 \text{ TeV}$ , we perform scans in the parameter space around the benchmark scenario we consider. We then study the feasibility to estimate the mass of the stau-LSP. We briefly discuss difficulties, which arise in the identification of hadronic tau decays due to small tau momenta and large particle multiplicities in our scenarios.

## I. INTRODUCTION

One of the main objectives of the experiments at the Large Hadron Collider (LHC) is to search for new phenomena beyond the Standard Model of particle physics (BSM) at and above the TeV energy scale. A well motivated scenario is the  $R$ -parity violating minimal supergravity model (mSUGRA) with baryon triality ( $B_3$ ) [1–5]. Contrary to the  $R$ -parity conserving mSUGRA model (also called the constrained MSSM) [6, 7], lepton number is violated. This leads to naturally light neutrino masses without introducing either a new see-saw energy scale at  $M_X = \mathcal{O}(10^{10} \text{ GeV})$  or new gauge-singlet superfields [3, 8–11]. However, within this model the lightest supersymmetric particle (LSP) is not stable. Thus the lightest neutralino is no longer a viable dark matter particle [90] and other candidates must be considered, such as the axino [13–16], gravitino [17–19], the lightest  $U$ -parity particle [20, 21] or slightly modified models like the NMSSM with a gravitino LSP [22]. More importantly for the focus of this paper, in this case, the LSP is no longer bounded by cosmology to be the lightest neutralino [23]. Any other supersymmetric particle is possible [24, 25]. This can lead to dramatically different signatures at colliders [26–28]. Within the  $B_3$  mSUGRA

model, certain non-neutralino LSP candidates are preferred [26, 29, 30]. In particular for small  $R$ -parity violating couplings the lightest scalar tau, the stau, is a possible LSP in large regions of the mSUGRA parameter space. This has been known for the  $R$ -parity conserving case for a long time, but has been discarded for the above cosmological reasons. In the  $R$ -parity violating case the stau is a natural LSP. We note however that the stau can also be the lightest supersymmetric particle within the ( $R$ -parity conserving) MSSM spectrum if one adds another (lighter) particle to the spectrum, like the gravitino. The stau then decays into this new particle and can be again consistent with cosmological observations; see e.g. Ref. [31].

In this paper, we consider in detail the discovery potential at the LHC for the  $B_3$  mSUGRA model with a stau LSP. We focus on the case of early data at 7 TeV center-of-mass energy. In order to be specific, we mainly restrict ourselves to one of the  $B_3$  mSUGRA benchmark points discussed in Ref. [32], as well as related scenarios. As we shall see, besides the good theoretical motivation, the stau LSP scenarios are also readily testable with early LHC data, because they can lead to a multi-lepton signature that is hard to achieve with the SM interactions.

The outline of the paper is as follows. In Sec. II, we present the model, which we investigate and then discuss in detail how a stau LSP can arise. We also review the benchmark scenario that is relevant for this work. An overview of all expected stau LSP signatures at the LHC is given in Sec. III, *i.e.* we consider the different dominating  $R$ -parity violating operators. We then present in Sec. IV in detail the particle multiplicities

<sup>\*</sup>desch@physik.uni-bonn.de

<sup>†</sup>Sebastian.Fleischmann@cern.ch

<sup>‡</sup>wienemann@physik.uni-bonn.de

<sup>§</sup>dreiner@th.physik.uni-bonn.de

<sup>¶</sup>sgrab@scipp.ucsc.edu

and kinematic properties of our benchmark scenario and for the most important SM backgrounds. Based on this, we develop in Sec. V a set of cuts that allow a discovery of these stau LSP scenarios with early LHC data. We employ a fast detector simulation and estimate systematic uncertainties in our analysis. We also investigate the possibility of reconstructing the stau LSP mass. Finally, we comment in Sec. VI on potential difficulties with tau identification due to the large particle multiplicities in our scenarios. We summarize and conclude in Sec. VII.

In App. A, we review some basic properties of the investigated benchmark scenario. We give an overview over different definitions of significances in App. B.

## II. THE $R$ -PARITY VIOLATING MSUGRA MODEL

### A. Motivation

In the  $B_3$  mSUGRA model [3, 6, 7] there are six free parameters at the unification scale ( $M_{\text{GUT}}$ )

$$M_0, M_{1/2}, A_0, \tan\beta, \text{sgn}(\mu), \mathbf{\Lambda}. \quad (1)$$

Here  $M_0, M_{1/2}$  are the universal supersymmetry breaking scalar and gaugino masses, respectively.  $A_0$  is the universal supersymmetry breaking scalar trilinear coupling and  $\tan\beta$  is the ratio of the two vacuum expectation values.  $\text{sgn}(\mu) = \pm 1$  is the sign of the Higgs mixing parameter. The magnitude of  $\mu$  as well as the respective bilinear scalar coupling  $B_0$  are fixed by radiative electroweak symmetry breaking [33]. In the  $B_3$  mSUGRA model the superpotential is extended beyond the MSSM by the following terms [24]

$$W_{B_3} = \lambda_{ijk} L_i L_j \bar{E}_k + \lambda'_{ijk} L_i Q_j \bar{D}_k + \kappa_i L_i H_2. \quad (2)$$

Here  $L_i, Q_i$  denote the lepton and quark  $SU(2)$  doublet superfields.  $H_2$  denotes the Higgs  $SU(2)$  doublet superfield which couples to the up-like quarks.  $\bar{E}_i, \bar{D}_i$  denote the lepton and quark  $SU(2)$  singlet superfields, respectively.  $i, j, k \in \{1, 2, 3\}$  are generation indices.  $\lambda_{ijk}$  denote nine (anti-symmetric in  $i \leftrightarrow j$ ),  $\lambda'_{ijk}$  twenty-seven dimensionless couplings.  $\kappa_i$  are three dimensional parameters, which vanish at the unification scale [3]. All the operators in Eq. (2) violate lepton number.

The parameter  $\mathbf{\Lambda}$  in Eq. (1) goes beyond the  $R$ -parity conserving mSUGRA model. It refers to a choice of *exactly one* of the thirty-six dimensionless couplings in Eq. (2) at a time.

$$\mathbf{\Lambda} \in \{\lambda_{ijk}, \lambda'_{ijk}\}, \quad i, j, k = 1, 2, 3. \quad (3)$$

Given one coupling at the unification scale, through the renormalization group equations (RGEs) other couplings are generated at the weak-scale ( $M_{EW}$ ) [34–36].

In principle, one can also choose more than one  $R$ -parity violating coupling at the unification scale. We mainly restrict ourselves to only one coupling, because it makes the investigation of the parameter space more manageable. However, our approach is also motivated from a phenomenological point of view, because experimental constraints on products of different  $R$ -parity violating couplings are in general more restrictive than on only a single coupling [12]. Furthermore, in the SM the top Yukawa is at least an order of magnitude larger than the other Yukawa couplings.

### B. Stau LSP

As mentioned above, in the  $B_3$  mSUGRA model the LSP is no longer constrained to be the lightest neutralino,  $\tilde{\chi}_1^0$ . Since the RGEs are modified compared to the  $R$ -parity conserving mSUGRA model by the interactions in Eq. (2), as well as the corresponding soft supersymmetry breaking terms, in principle new LSPs may arise as a function of the input parameters in Eq. (1). For large values of specific couplings, *i.e.*  $\mathbf{\Lambda} \gtrsim \mathcal{O}(10^{-2})$ , this does in fact happen

$$\begin{aligned} \tilde{\mu}_R & \text{ for large } \lambda_{132}, \\ \tilde{\nu}_i & \text{ for large } \lambda'_{ijk}, \\ \tilde{e}_R & \text{ for large } \lambda_{121}, \lambda_{131}, \lambda_{231}. \end{aligned} \quad (4)$$

as discussed in detail in Ref. [26, 29, 30]. The relevant couplings are given here in parentheses. However, even for small values of arbitrary couplings there are large regions of parameter space, where the lightest stau,  $\tilde{\tau}_1$ , is the LSP. This occurs for large values of  $M_{1/2}$  (which drives up the  $\tilde{\chi}_1^0$  mass faster than the stau mass) and small values of  $M_0$ ; see App. A2 for the  $\tan\beta$  dependence. For a fixed value of  $M_0$  there is always a value of  $M_{1/2}$  above which the stau is the LSP [32]. For example, at  $A_0 = -100$  GeV,  $\tan\beta = 10$  and  $\text{sgn}(\mu) = +1$  the region is approximately given by

$$\tilde{\tau}_1 - \text{LSP} : \quad M_{1/2} \gtrsim 3.8 \cdot M_0 + 175 \text{ GeV}. \quad (5)$$

It is the purpose of this paper to study in detail the detectability of stau LSP models with early LHC data.

There is a series of papers in the literature on a stau LSP [3, 10, 27, 32, 37–49]. To the best of our knowledge a stau LSP was first considered in Ref. [37] in a bilinear  $R$ -parity breaking model with a focus on charged Higgs phenomenology [91]. There has been further work on a stau LSP in bilinear  $R$ -parity violating models [39, 44, 48]. In Ref. [44], LHC phenomenology is considered in some detail, however the focus is on a  $\tilde{\chi}_1^0$  LSP, with only peripheral mention of the stau LSP discovery reach. In Ref. [40] the decay lengths of slepton LSPs are considered in both bilinear and trilinear  $R$ -parity violating models. LEP II searches for a stau LSP were performed in Refs [45–47], allowing only for two-body  $R$ -parity violating decays of the

	BC1	BC2	BC3
Operator	$\lambda_{121} L_1 L_2 \bar{E}_1$	$\lambda'_{311} L_3 Q_1 \bar{D}_1$	$\lambda'_{331} L_3 Q_3 \bar{D}_1$
Coupling (@ $M_{GUT}$ )	0.032	$3.5 \cdot 10^{-7}$	0.122
Coupling (@ $M_{EW}$ )	0.048	$1.1 \cdot 10^{-6}$	0.344
LSP	$\tilde{\tau}_1$	$\tilde{\tau}_1$	$\tilde{\nu}_\tau$
$M_0$ (GeV)	0	0	100
$M_{1/2}$ (GeV)	400	400	250
$\tan \beta$	13	13	10
$A_0$ (GeV)	0	0	-100

TABLE I: The main properties of the  $B_3$  mSUGRA benchmark points.

stau. Recently, Ref. [43] investigated stau LSP scenarios, where the stau decays leptonically via 2-body decays. It was shown that these scenarios might already be discovered in early LHC data via same-sign trilepton events.

In Ref. [3] the  $B_3$  mSUGRA model was constructed. It was shown that extensive regions of parameter space lead to a stau LSP. Furthermore it was shown that in some regions of parameter space the stau dominantly decays via 2-body decays and in others via 4-body decays. In Ref. [32] benchmarks were defined for exemplary phenomenological and experimental analyses, for both the 2-body and 4-body decays. These are discussed below. In Ref. [27], the origin of the 2-body and 4-body decays from the RGEs was studied in detail. The example of resonant slepton production was then analyzed in the case of a stau LSP.

We here present for the first time a comprehensive analysis at the LHC of stau LSP scenarios. We focus mainly on one specific benchmark point BC1 [32]. For this we investigate the signal and the background in great detail. We include a fast detector simulation using the program package `Delphes` [50].

### C. Benchmark Scenarios

In Ref. [32] four Bonn–Cambridge (BC) benchmark points for studying  $R$ -parity violating models in detail were defined. BC1–BC3 are  $B_3$  mSUGRA models, BC4 involves a baryon number violating operator. The main properties of the points BC1–BC3 are summarized in Table I. BC1 and BC2 have a stau LSP, the focus of our investigation here. In contrast to BC2, BC1 involves an additional purely leptonic

operator,  $\lambda_{121} L_1 L_2 \bar{E}_1$ . Thus the  $\tilde{\chi}_1^0$  and stau decay purely leptonically. In the production and cascade decay of squarks and gluinos at the LHC this leads to many leptons in the final state. In BC2 the stau LSP decays purely hadronically, leading to significantly less final state leptons. Here we focus on the BC1 scenario, due to the better prospects of early discovery at the LHC. The mass spectrum as well as the dominant decay branching fractions for BC1 are given in App. A.

### III. STAU LSP SIGNATURES AT THE LHC

As a first step of our analysis, we classify the main LHC signatures, assuming that the stau decay is dominated by only one  $R$ -parity violating operator, *cf.* Eq. (2). For simplicity we focus on the cascade process

$$qq/gg \rightarrow \tilde{q}\tilde{q} \rightarrow jj\tilde{\chi}_1^0\tilde{\chi}_1^0 \rightarrow jj\tau\tau\tilde{\tau}_1\tilde{\tau}_1, \quad (6)$$

where  $\tilde{q}$  is a squark, and  $j$  denotes a jet. The final-state staus can only decay via  $R$ -parity violating operators. We then classify the signatures according to the possible stau decays. The results are summarized in Tables II, III, and IV, for the operators  $L_i L_j \bar{E}_k$ ,  $L_i Q_j \bar{D}_k$ , or  $\bar{U}_i \bar{D}_j \bar{D}_k$  [92], respectively. Here we assume that always only one operator is dominant [93]. In the left column we denote the dominant coupling, in the middle column, the corresponding dominant 2- or 4-body stau decays. The resulting final state signatures for the cascade of Eq. (6) are given in the right column. Here  $\ell$  denotes an electron or muon,  $\tau$  a tau and  $\cancel{E}_T$  missing transverse energy due to neutrinos in the final state. We have not included neutrinos from tau decays.

We show in Fig. 1 as an example the 4-body stau LSP decay into  $\tau^+ \mu^+ e^- \bar{\nu}_e$  via  $\lambda_{121}$ , *cf.* the first decay in Tab. II. The stau does not directly couple to the  $L_1 L_2 \bar{E}_1$  operator and thus first couples to a virtual neutralino radiating off a tau lepton. The neutralino then couples to, for example, an electron anti-neutrino and a virtual electron sneutrino,  $\tilde{\nu}_e$ , which decays via  $\lambda_{121}$  into an electron and a muon. We end up with a 4-body decay of the stau LSP.

We observe that the partial width,  $\Gamma_4$ , for the 4-body decay gets suppressed if the sfermion (gaugino) masses increase, *i.e.* the behavior is approximately  $\Gamma_4 \sim m_{\tilde{f}}^{-4} (m_{\tilde{\chi}_1^0}^{-2})$  [3]. Furthermore, we see that for the scenario BC1, the decay is mainly mediated by the  $\tilde{\chi}_1^0$ . The (mainly right-handed stau LSP) couples much stronger to the (bino-like)  $\tilde{\chi}_1^0$  than to the heavier (wino- and higgsino-like) neutralinos. If we also take into account the Majorana nature of the neutralinos we obtain from Fig. 1 the second stau LSP decay mode of Tab. II.

The stau LSP can in principle also decay via a virtual chargino instead of a virtual neutralino. However, these decays are suppressed by several orders of magnitude. On the one hand, they are suppressed due to

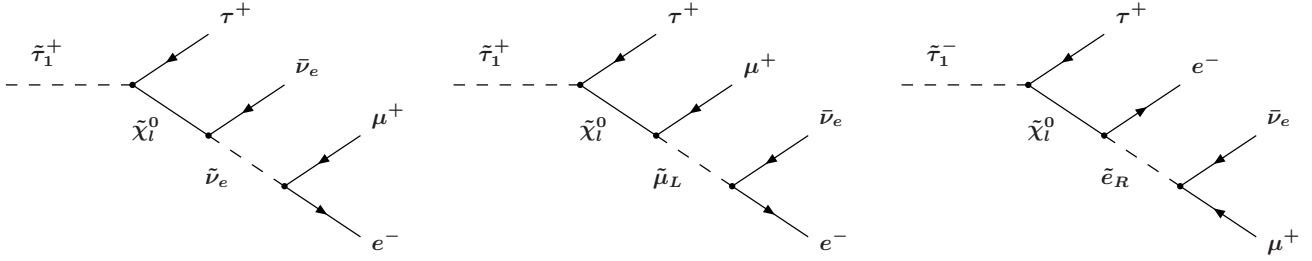


FIG. 1: Feynman diagrams contributing to the 4-body stau LSP decay  $\tilde{\tau}_1^+ \rightarrow \tau^+ \mu^+ e^- \bar{\nu}_e$  via  $\lambda_{121}$ . In this example, the stau LSP decays via a virtual neutralino  $\tilde{\chi}_l^0$  ( $l = 1 \dots 4$ ). In addition, the first, second and third diagram involve a virtual electron sneutrino,  $\tilde{\nu}_e$ , a virtual (left-handed) smuon,  $\tilde{\mu}_L$ , and a virtual  $\mu$  right-handed selectron,  $\tilde{e}_R$ , respectively.

coupling	$\tilde{\tau}_1^+$ decay	LHC signature
$\lambda_{121} = -\lambda_{211}$	$\tau^+ \mu^+ e^- \bar{\nu}_e$ $\tau^+ \mu^- e^+ \nu_e$ $\tau^+ e^+ e^- \bar{\nu}_\mu$ $\tau^+ e^- e^+ \nu_\mu$	$2j + 4\tau + 4\ell + \cancel{E}_T$
$\lambda_{122} = -\lambda_{212}$	$\tau^+ \mu^+ \mu^- \bar{\nu}_e$ $\tau^+ \mu^- \mu^+ \nu_e$ $\tau^+ e^+ \mu^- \bar{\nu}_\mu$ $\tau^+ e^- \mu^+ \nu_\mu$	with $\ell = e, \mu$
$\lambda_{131} = -\lambda_{311}$	$e^+ \nu_e$	$2j + 2\tau + 2\ell + \cancel{E}_T$
$\lambda_{132} = -\lambda_{312}$	$\mu^+ \nu_e$	
$\lambda_{231} = -\lambda_{321}$	$e^+ \nu_\mu$	
$\lambda_{232} = -\lambda_{322}$	$\mu^+ \nu_\mu$	
$\lambda_{123} = -\lambda_{213}$	$\mu^+ \bar{\nu}_e$ $e^+ \bar{\nu}_\mu$	$2j + 2\tau + 2\ell + \cancel{E}_T$ $2j + 3\tau + 1\ell + \cancel{E}_T$
$\lambda_{133} = -\lambda_{313}$	$e^+ \bar{\nu}_\tau$ $\tau^+ \bar{\nu}_e$ $\tau^+ \nu_e$	
$\lambda_{233} = -\lambda_{323}$	$\mu^+ \bar{\nu}_\tau$ $\tau^+ \bar{\nu}_\mu$ $\tau^+ \nu_\mu$	$2j + 4\tau + \cancel{E}_T$

TABLE II: Scenarios assuming one non-vanishing  $L_i L_j \bar{E}_k$  operator. The column in the middle shows the possible stau LSP decays, for the  $\lambda_{ijk}$  couplings in the left column. The right column shows the resulting LHC signatures. The SUSY cascade  $q\bar{q}/g\bar{g} \rightarrow \tilde{q}\tilde{q} \rightarrow jj\tilde{\chi}_1^0\tilde{\chi}_1^0 \rightarrow jj\tau\tau\tilde{\tau}_1\tilde{\tau}_1$  has been assumed. Note that gluino,  $\tilde{g}$ , pair production instead of squark pair production will usually give two additional jets; for example via the decay  $\tilde{g} \rightarrow j\tilde{q}$ .

heavy propagators. On the other hand, the (mainly right-handed) stau couples in mSUGRA more strongly to the (bino-like)  $\tilde{\chi}_1^0$  than to the (wino-like)  $\tilde{\chi}_1^\pm$ .

Note, that due to the Majorana nature of the  $\tilde{\chi}_1^0$ , every charge combination of the two staus is possible. The flavor and charge of the leptons and quarks in the final state, are determined via the different decay modes of the stau LSP.

In general, more complicated decay chains than Eq. (6) can occur, leading typically to additional fi-

coupling	$\tilde{\tau}_1^+$ decay	LHC signature
$\lambda'_{1jk}$	$\tau^+ \bar{u}_j \bar{d}_k e^+$ $\tau^+ u_j \bar{d}_k e^-$ $\tau^+ \bar{d}_j \bar{d}_k \bar{\nu}_e$ $\tau^+ d_j \bar{d}_k \nu_e$	$6j + 4\tau + \ell\ell$ $6j + 4\tau + \ell + \cancel{E}_T$
$\lambda'_{2jk}$	$\tau^+ \bar{u}_j \bar{d}_k \mu^+$ $\tau^+ u_j \bar{d}_k \mu^-$ $\tau^+ d_j \bar{d}_k \bar{\nu}_\mu$ $\tau^+ d_j \bar{d}_k \nu_\mu$	$6j + 4\tau + \cancel{E}_T$
$\lambda'_{3jk}$	$u_j \bar{d}_k$	$6j + 2\tau$

TABLE III: Same as Tab. II but for one non-vanishing  $L_i Q_j \bar{D}_k$  operator.

coupling	$\tilde{\tau}_1^+$ decay	LHC signature
$\lambda''_{ijk}$	$\tau^+ u_i d_j \bar{d}_k$ $\tau^+ \bar{u}_i \bar{d}_j \bar{d}_k$	$8j + 2\tau$

TABLE IV: Same as Tab. II but for one non-vanishing  $\bar{U}_i \bar{D}_j \bar{D}_k$  operator.

nal state particles. The most important are:

- Additional jets from the production of gluinos and their subsequent decays into squarks and quarks.
- Additional leptons from decays involving heavy neutralinos and charginos. For example, a left-handed squark might decay to a  $\tilde{\chi}_2^0$  or  $\tilde{\chi}_1^+$ , which then decays to a lepton and a slepton.
- Additional leptons from the decay of a  $\tilde{\chi}_1^0$  next-to-next-to-next-to LSP (NNNLSP) into right-handed selectrons or smuons, *i.e.*  $\tilde{\chi}_1^0 \rightarrow \ell^\pm \tilde{\ell}_R^\mp$  followed by  $\tilde{\ell}_R^\pm \rightarrow \ell^\pm \tau^\pm \tilde{\tau}_1^\mp$ .

The last process is special for stau LSP scenarios. Within mSUGRA, it is kinematically only allowed if  $M_{1/2} \gg M_0$ , *e.g.* for  $M_{1/2} > 400$  GeV for  $M_0 = 0$  GeV. Note, that  $M_{1/2}$  increases the mass of the (bino-like)  $\tilde{\chi}_1^0$  faster than the mass of the  $\tilde{\ell}_R$  [51]. If these new decay channels are open, we can have two addi-

tional taus and four additional electrons or muons in the final state. See Ref. [27] for explicit examples.

The multi charged lepton final states (especially electrons and muons) are the most promising signatures to be tested with early LHC data. It is relatively easy to identify electrons and muons in the detector and for high multiplicities the SM background is very low [56]. In the next section, we therefore investigate the discovery potential of stau LSP scenarios, where the stau decays in the 4-body decay mode via the operator  $\lambda_{121}L_1L_2\bar{E}_1$ , leading to a maximal number of muons and electrons in the final state, *cf.* Tab. II. We also analyze the potential of reconstructing the mass of the stau LSP, once a discovery has been made.

Note, that scenarios, where the stau decays via a 2-body  $L_iL_j\bar{E}_k$  mode ( $i, j$  or  $k = 3$ ) might have a similar discovery potential, because the charged leptons have on average larger momenta. We also expect larger values of  $\cancel{E}_T$ , because a 2-body stau decay via  $L_iL_j\bar{E}_k$  involves always one neutrino, *cf.* Tab. II.

If the stau LSP couples mainly to a  $L_iQ_j\bar{D}_k$  operator, there are (at parton level) at least six jets and two taus in the final state, *cf.* Tab. III. Furthermore, for  $i = 1, 2$ , there are possibly one or two additional charged electrons or muons as well as four additional taus. Again, due to the Majorana nature of the  $\tilde{\chi}_1^0$ , all charge combinations for these electrons and muons are possible, leading for example to like sign dilepton events. Unlike the scenarios shown in Tab. II ( $L_iL_j\bar{E}_k$ ), the scenarios in Tab. III ( $L_iQ_j\bar{D}_k$ ) do not necessarily lead to  $\cancel{E}_T$  (apart from neutrinos from tau decays). It should therefore be possible to directly reconstruct the mass peaks of sparticles, especially the stau LSP. However, combinatorial backgrounds due to the many jets in the final state complicate this task.

A special case arises if the  $L_iQ_j\bar{D}_k$  operator involves quark superfields of the third generation, *i.e.*  $j$  or  $k = 3$ . For  $k = 3$  two jets in the final states are  $b$ -jets, one from each stau decay. For  $i = 1, 2$  and  $j = 3$  the situation is similar. We also obtain one  $b$ -jet from nearly each stau LSP decay. However, decays which involve an electron or muon are now kinematically suppressed or forbidden due to a top quark in the final state, *cf.* Tab. III. Finally, for a non-vanishing coupling  $\lambda'_{33k}$ , the stau might only decay via a 3-body mode and a virtual top-quark. See Ref. [27] for details.

In this paper, we focus on stau LSP scenarios with a lepton-number violating  $L_iL_j\bar{E}_k$  operator. However, we briefly discuss signatures, which arise from a non-vanishing baryon-number violating operator  $\bar{U}_i\bar{D}_j\bar{D}_k$ .

We see in Tab. IV that a non-vanishing  $\lambda'_{ijk}$  coupling leads mainly to a 4-body decay of the stau LSP, resulting in at least eight parton level jets and four taus in the final state. Due to the many jets, we expect tau identification via its hadronic decay modes to be very difficult; see Sec. VI. A jet from a cascade decay might overlap with the tau jet. Furthermore, the

three jets in a stau decay can be boosted such that they might appear as only one jet. However, these jets might still be revealed by investigating the substructure of jets. See Ref. [52] for  $\tilde{\chi}_1^0$  LSP scenarios, with purely hadronic ( $\bar{U}_i\bar{D}_j\bar{D}_k$ ) LSP decays. See also Refs. [53–57] for related work. We expect that similar techniques will work for stau LSP scenarios.

For the special case of  $j$  or  $k = 3$ , the baryon-number violating stau decays lead to two  $b$ -jets in the final state. For  $i = 3$ , the final state up-type quark in Tab. IV will be a top-quark. If the decay into a top quark is kinematically forbidden, the stau LSP might decay in a 5-body decay via a virtual top.

#### IV. SIMULATION OF SIGNAL AND BACKGROUND

In this section we perform a full Monte Carlo analysis of the stau LSP benchmark scenario BC1 (with  $\lambda_{121} = 0.032$  at  $M_{GUT}$ ; *cf.* Tab. I) and the dominant SM backgrounds. Our signal process is pair production of all SUSY particles. We also employ fast detector simulations. The mass spectrum and branching ratios (BRs) of BC1 are given in App. A.

##### A. Major Backgrounds

In what follows, we only consider SM backgrounds that can lead to at least one (parton level) electron, muon or tau in the final state. Furthermore, we expect from most of the SUSY (signal) events additional energy in the form of hard jets, that arise from decays in the upper parts of the decay chain.

We thus consider the following SM processes as the major backgrounds in our analysis:

- $t\bar{t}$  production.
- $Z$  + jets. The  $Z$  can decay into a pair of charged leptons. Because the SUSY events possess additional large amounts of energy from jets, we only consider  $Z$  production with at least one hard jet at parton level.
- $W$  + jets. The  $W$  can decay into a charged lepton and a neutrino. In order for the  $W$  production to be competitive with the SUSY processes, we demand at least two additional hard jets at parton level [58].
- Di-boson ( $WW$ ,  $WZ$  and  $ZZ$ ) production [94].

Table V gives an overview of the background samples used in our analysis. QCD di- and multi-jet events have been neglected. It has been shown *e.g.* in Ref. [60] that QCD background can efficiently be suppressed in multi-lepton final states.

Sample	sub-sample	simulated events	Generator	comments
$t\bar{t}$		240 000	MC@NLO + Jimmy/Herwig	
$Z$ + jets	$Z \rightarrow e^+e^- + \geq 1$ jet	222 000	Alpgen + Jimmy/Herwig	for each process split in the exclusive samples 1, ..., 4 extra partons and the inclusive sample $\geq 5$ extra partons
	$Z \rightarrow \mu^+\mu^- + \geq 1$ jet	231 000		
	$Z \rightarrow \tau\tau + \geq 1$ jet	232 000		
$W$ + jets	$W \rightarrow e\nu + \geq 2$ jets	518 000	Alpgen + Jimmy/Herwig	for each process split in the exclusive samples 2, ..., 4 extra partons and the inclusive sample $\geq 5$ extra partons
	$W \rightarrow \mu\nu + \geq 2$ jets	642 000		
	$W \rightarrow \tau\nu + \geq 2$ jets	659 000		
di-boson	$WW$	30 000	Jimmy/Herwig	
	$WZ$	20 000		
	$ZZ$	9 990		
signal		$\approx 10\,000$ each	Jimmy/Herwig	

TABLE V: Monte Carlo samples of the SM background and signal events used for our analysis. The third column shows the number of simulated events (for the `Alpgen` samples after MLM matching [71–73]) and the fourth column shows the employed generators. For the simulation of the signal we employed a special version of `Herwig` which also incorporates the 4-body decays of the stau LSP [67]. Note, that we simulated approximately 10 000 signal events for each mSUGRA parameter point in Sec. VB including BC1.

## B. Simulation and Selection Cuts

The SUSY mass spectra were calculated with `SOFTSUSY3.0` [61, 62]. The `SOFTSUSY` output was fed into `ISAWIG1.200` and `ISAJET7.75` [63] in order to calculate the decay widths of the SUSY particles (beside the stau LSP). The signal processes, *i.e.* pair production of SUSY particles, was simulated with a modified version of `Herwig6.510` [64–66] which also simulates the 4-body decays of the stau LSP [67]. We employed `Jimmy4.31` [68] to simulate the underlying event.

The  $t\bar{t}$  background was simulated with `MC@NLO3.41` [69, 70], the di-boson background in `Herwig6.510`. We used `Alpgen2.13` [71–73] interfaced with `Herwig6.510` to simulate the  $Z$ +jets and  $W$ +jets backgrounds. We also employed `Jimmy4.31` in all cases for modeling of the underlying event. All Monte Carlo samples are based on the parton distribution functions given by `CTEQ6L1` [74]. The employed Monte Carlo generators are also summarized in Table V.

Detector effects on signal and background were accounted for using the generic detector simulation `Delphes1.8` [50]. Its detector settings were tuned to an ATLAS-like detector at the LHC [95]. The results of the detector simulation were cross checked with the `PGS4` simulation [76] using its generic LHC tune. A sufficient agreement of the two codes was observed for most observables. However, the identification of electrons and especially tau leptons showed some discrepancies, *cf.* Sec. VI. Detector simulations with full detail of the calorimetry and tau identification algorithms need to be done to get more reliable results. In the comparison between `PGS` and `Delphes` we observe some shifts in the energy scale especially for electrons in our signal events. Using the differences between the two fast simulations as an estimate for the energy scale uncertainty would lead to unreasonably large systematic uncertainties in the estimate of the expected discovery significance. Instead, we take an estimate of

the ATLAS collaboration [60] for the expected background uncertainties to calculate significances in the following.

particle	transverse momentum	pseudorapidity
electron	$p_T > 7$ GeV	$ \eta  < 2.5$
muon	$p_T > 6$ GeV	$ \eta  < 2.7$
tau	$p_T > 10$ GeV	$ \eta  < 2.5$
jet	$p_T > 20$ GeV	$ \eta  < 5.0$

TABLE VI: Cuts for the particle selection for the signal and background.

The particle selection was guided by the definitions used by the ATLAS collaboration for SUSY studies, *cf.* Ref. [60, pp. 1518]. The selection cuts are given in Tab. VI. We similarly followed these guidelines for the overlap removal of reconstructed objects. This is needed, because a single particle may be reconstructed as several different objects.

For the overlap removal we simply use the distance in pseudorapidity  $\eta$  and azimuthal angle  $\phi$ , defined as  $\Delta R = \sqrt{(\Delta\phi)^2 + (\Delta\eta)^2}$ . Objects are selected in the following order:

1. Muons, if no jet and no previously selected muon is present within  $\Delta R < 0.4$ .
2. Electrons, if no jet is present within  $0.2 < \Delta R < 0.4$  and no previously selected electron within  $\Delta R < 0.4$ .
3. Hadronically decayed taus, if no electron or tau has already been selected within  $\Delta R < 0.4$ .
4. Jets, if no electron, tau or another jet has already been selected within  $\Delta R < 0.4$ .

These cuts take care of the fact that electrons and taus are usually also reconstructed as jets. Furthermore, electrons are more reliably identifiable than taus. In

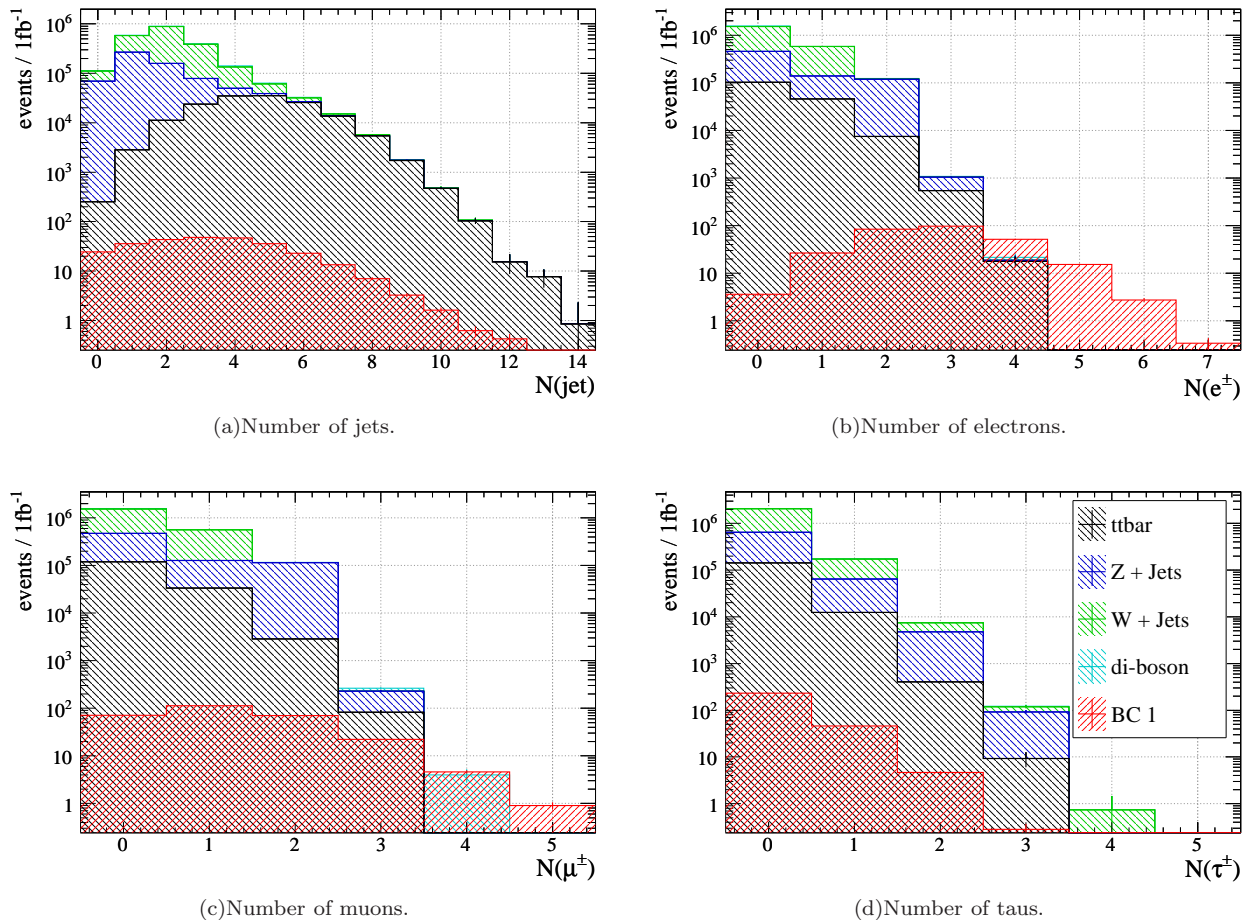


FIG. 2: The number of reconstructed particles per event after selection cuts and overlap removal as described in Sec. IV B. The color code for the curves in all four plots is given in (d). The different background contributions are stacked on top of each other, while the expected signal is shown in front of the histograms in red. The signal corresponds to the benchmark scenario BC1 [32]. The number of events are scaled to  $1 \text{ fb}^{-1}$  at  $\sqrt{s} = 7 \text{ TeV}$ .

addition, one does not want to select electrons or muons, that stem from heavy flavor decays within jets.

### C. Particle Multiplicities and Kinematic Properties

In this section we show the basic kinematic properties of the BC1 scenario compared to the most important Standard Model backgrounds. We also motivate the cuts to obtain a good significance and a good signal over background ratio. No further event selection cuts beyond the object selection cuts given in Sec. IV B are applied here. All samples are scaled to an integrated luminosity of  $1 \text{ fb}^{-1}$  at a center-of-mass energy of  $\sqrt{s} = 7 \text{ TeV}$ .

We show in Fig. 2 the number of reconstructed jets, electrons, muons and taus, respectively. The different background contributions are stacked on top of each other, while the expected BC1 signal is shown in front of the background histograms. Error bars correspond

to statistical uncertainties of the generated samples. From the discussion in Sec. III we expect 2-4 jets at parton level for the scenario BC1. This behavior can also be seen in Fig. 2(a) (red histogram), where the signal distribution is maximal at 3 jets. In general, we can get in addition to the parton-level jets also jets from parton shower radiation and possibly from non-identified hadronically decaying taus.

According to Fig. 2(a) the SM background is predominant even for high jet multiplicities. The  $t\bar{t}$  background contributes via the two (parton-level)  $b$ -jets from top decays as well as jets from a hadronically decaying  $W$ . Therefore, a  $b$ -jet veto may in principle suppress this background. However, the signal can contain  $b$ -jets as well, and we will not consider  $b$ -tagging in our analysis.

The bins in Fig. 2(a) with  $\leq 1$  jet are dominated by the  $Z + \geq 1$  jet background (blue histogram). This is expected due to the large  $Z$  + jets cross section. Note that Fig. 2(a) displays the event numbers on a logarithmic scale. In contrast,  $W$  + jets (green histogram)

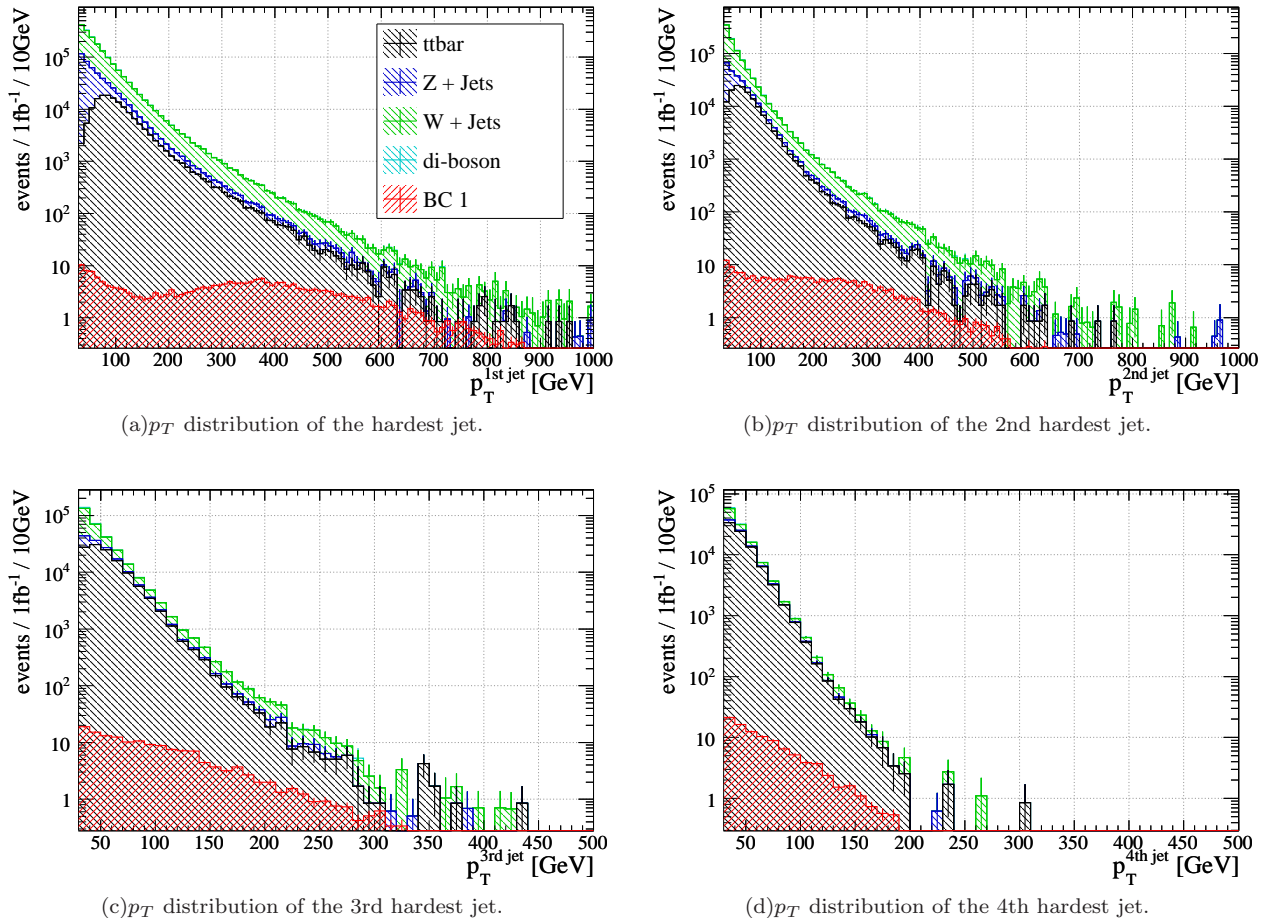


FIG. 3:  $p_T$  distributions of the four hardest jets after object selection cuts and overlap removal.

mostly dominates for  $\geq 2$  jets, because we only show  $W$  production in association with two parton-level jets in Fig. 2(a).

The transverse momentum,  $p_T$ , distributions of the four hardest jets are shown in Fig. 3. We observe in Fig. 3(a) that the  $p_T$  distribution of the hardest signal jet is relatively flat over several hundreds of GeV whereas the distribution of the background falls off steeply. One can also see a peak in the  $p_T$  distribution of the signal around 360 GeV. This peak is due to the mainly hard jets from the decay of a squark into the  $\tilde{\chi}_1^0$ . Note that the mass difference between most of the squarks and the  $\tilde{\chi}_1^0$  in BC1 is 400-500 GeV, *cf.* App. A. The invariant mass of the hardest jet with the decay products of the  $\tilde{\chi}_1^0$  might thus allow a reconstruction of the squark masses.

Gluginos decaying into a jet and a squark will in general produce softer jets, because the respective mass difference is only  $\approx 100$  GeV. Therefore, these additional jets are most probably found in Fig. 3(b)–3(d).

We see in Fig. 3 that the signal over background ratio improves if one only allows for very hard jets. This is also reflected by the visible hadronic mass,

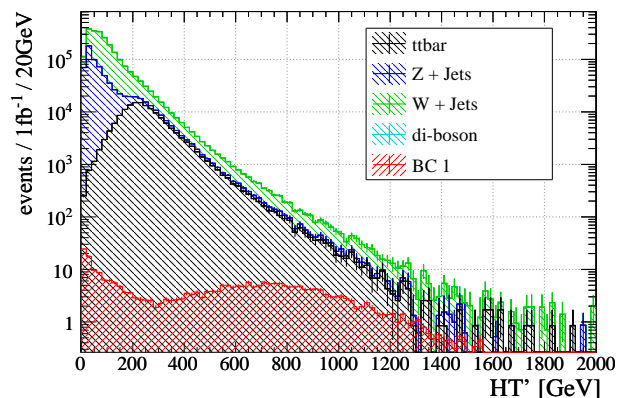


FIG. 4: The number of events per  $1\text{fb}^{-1}$  as a function of the scalar sum of the transverse momenta of the four hardest jets,  $HT'$ , after object selection cuts and overlap removal.

$HT' = \sum_{\text{jet } 1-4} p_T$ , which is the scalar sum of the transverse momenta of the four hardest jets. The respective distribution is given in Fig. 4. Note, that this cut alone (no actual cut is defined at this point) would



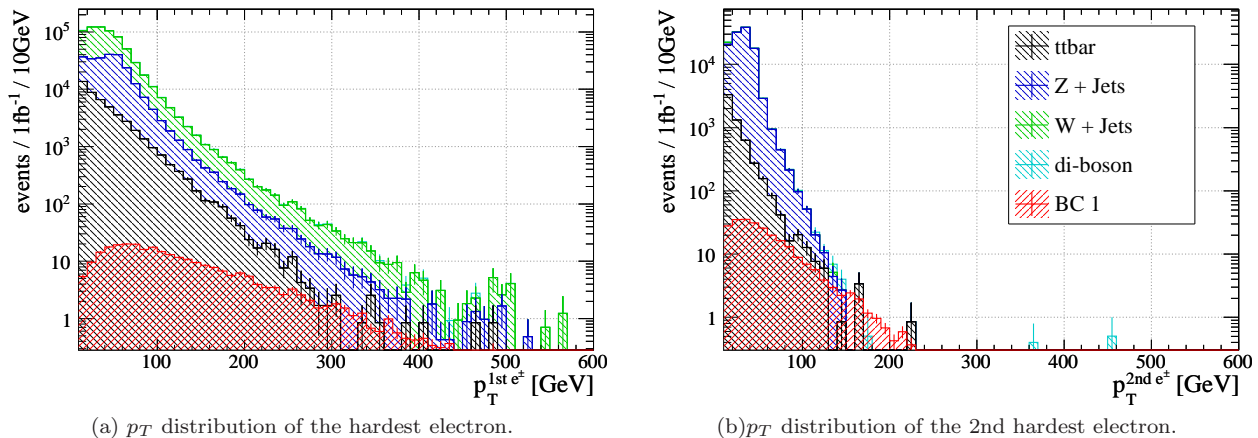


FIG. 5:  $p_T$  distributions of the two hardest electrons after object selection cuts and overlap removal.

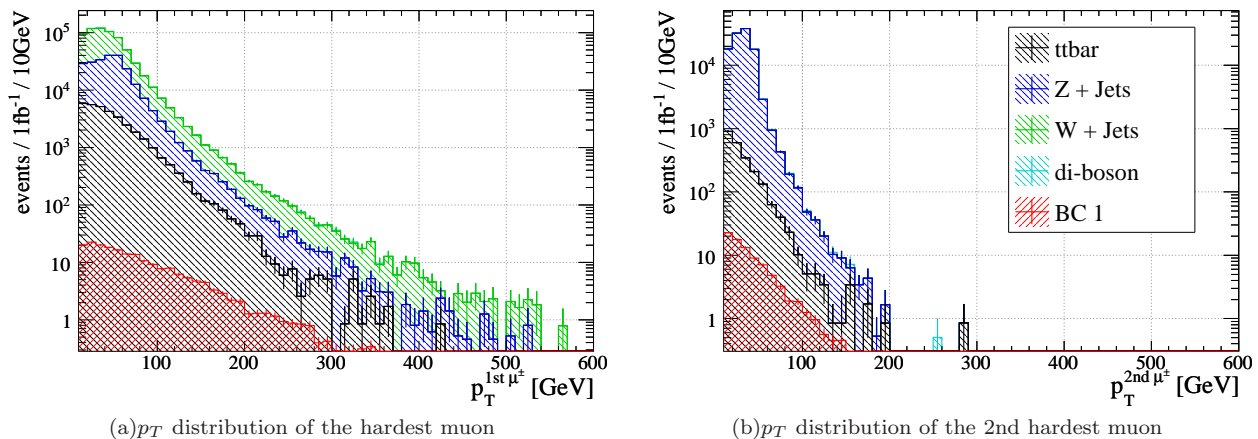


FIG. 6:  $p_T$  distributions of the two hardest muons after object selection cuts and overlap removal.

still give an overwhelming amount of QCD background events. We thus need to also make use of the charged leptons in the final state.

The most striking signature of the BC1 scenario is the large number of electrons and muons in the final state. We show the respective multiplicities in Fig. 2(b) and Fig. 2(c). Even with an integrated luminosity of only  $1 \text{ fb}^{-1}$  at  $\sqrt{s} = 7 \text{ TeV}$ , we expect several dozen events with four or more electrons in the final state!

The signal distribution of the number of reconstructed electrons peaks at 3 whereas for the muons it peaks at 1. This is exactly the expected behavior from the parton-level signatures reviewed in Sec. III, *cf.* especially the row for  $\lambda_{121}$  in Tab. II. The decay of two stau LSPs in a typical BC1 event leads at parton level to 2–4 electrons and 0–2 muons. Furthermore, additional electrons or muons can arise from other particle decays; *e.g.* in BC1 from leptonic tau decays.

It is interesting to note that the ratio of the number of reconstructed electrons and muons carries infor-

mation about the involved  $B_3$  coupling. Comparing Fig. 2(b) with 2(c), we see that the ratio of the average number of electrons to muons is roughly three. This is because  $\lambda_{121}$  couples two lepton superfields of the first generation to one of the second generation. Thus, stau LSP decays produce more electrons than muons, *cf.* Tab. II. If we instead had  $\lambda_{122} \neq 0$ , the situation would be reversed (modulo differences due to the reconstruction efficiencies).

According to Fig. 2(b), it is possible to obtain a nearly background free sample by requiring more than four electrons in the final state! However, such a cut would also veto most of the signal events and is therefore not well suited for a study of early data. Furthermore, electrons can easily be faked by early photon conversions or low multiplicity jets. Therefore, we demand (as a cut in the next section) “only” the presence of at least one electron with  $p_T > 32 \text{ GeV}$ , another electron with  $p_T > 7 \text{ GeV}$  and at least one muon with  $p_T > 40 \text{ GeV}$  in the final state. It is hard for the QCD background to fake an electron and a muon at the same time. In addition only the leptonically decay-

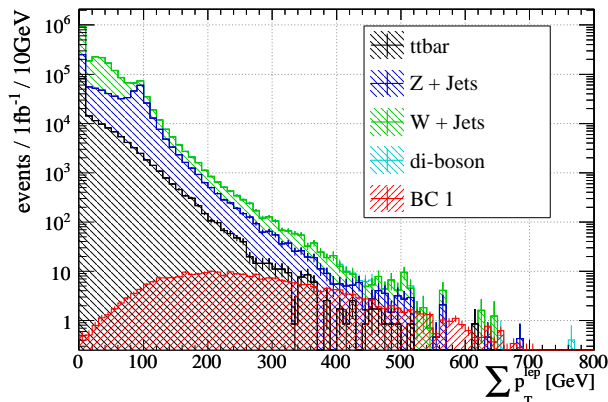


FIG. 7: The number of events per  $10 \text{ fb}^{-1}$  as a function of the scalar sum of the transverse momenta of electrons and muons,  $\sum p_T^{\ell}$ , after object selection cuts and overlap removal.

ing  $W$ s from  $t\bar{t}$  production, leptonically decaying taus from  $Z \rightarrow \tau\tau$  production, and di-boson production can lead to an electron *and* a muon at parton level. We thus expect a strong suppression of the background from this cut, *cf.* Tab. VII.

We display the  $p_T$  distributions of the two hardest electrons in Fig. 5 and those of the two hardest muons in Fig. 6. The  $p_T$  distribution of the background falls off more rapidly than the signal. In Fig. 5(b), we see that for  $p_T > 150$  GeV the signal even dominates over the background.

Due to their large multiplicity and large transverse momenta, leptons beyond the sub-leading electron and leading muon can contribute significantly to the energy deposition of all leptons. The cut  $\sum p_T^{\ell} > 230$  GeV, which we employ in the next section, accounts for the fact that the signal lepton  $p_T$ s are on average larger than the background. The lepton momenta are large because they lie at the end of a decay chain of heavy SUSY particles, *cf.* Tab. VIII. Note, that  $\sum p_T^{\ell}$  is the  $p_T$  sum of all electrons and muons. The distribution is shown in Fig. 7.

We show in Fig. 2(d) the multiplicity of reconstructed (hadronically decaying) taus. The signal distribution peaks at 0. At first glance this is surprising, because from Tab. II we expect 4 taus in most of the BC1 SUSY events.

However, with respect to tau identification (ID), the topologies in BC1 (*cf.* Sec. III) are special. Due to a large number of taus and jets from the SUSY decay chains, overlaps between different tau jets and other jets make standard tau ID via its hadronic decays very difficult. The low visible momentum of many tau leptons in this scenario complicates the tau lepton identification further. As we show in more detail in Sec. VI, tau ID in BC1 has an efficiency of at best 20%-30%. The exact number depends on the working point on the efficiency-vs-rejection curve of the tau ID

algorithm, that is used. Furthermore, we observe a strong dependence on the nature of the fast detector simulation used, *i.e.* Delphes or PGS4 (*cf.* Fig. 17). In any case the ID efficiency is expected to be a factor of 2–3 smaller in BC1, than *e.g.* in  $Z \rightarrow \tau\tau$  events, even for tau leptons of the same momentum.

Although the number of parton-level taus is much larger in BC1 compared to the SM backgrounds, this does no longer hold for the reconstructed taus. This can also be seen in Fig. 8, where we display the (visible)  $p_T$  of the two hardest identified taus. Even for large momenta, the background always exceeds the signal. Naively, we would expect the contrary. Like the electrons, Fig. 5, the taus result from the decay chains of heavy SUSY particles. In addition, the tau leptons in BC1 are mostly very soft, which reduces the ID efficiency further. Therefore, we do not employ the tau to improve the signal to background ratio.

In Fig. 9 we present the missing transverse energy distribution for the signal and the backgrounds. Even though we investigate a  $B_3$  scenario, where the LSP does not escape detection, the missing transverse energy,  $\cancel{E}_T$ , can be significant in BC1. For example, a cut on the missing energy of  $\cancel{E}_T > 400$  GeV improves the signal over  $t\bar{t}$  background ratio from initially  $\mathcal{O}(0.001)$  to  $\mathcal{O}(1)$ , *cf.* Fig. 9.

The reason for this are the neutrinos from the stau LSP decays

$$\begin{array}{c} \tilde{\chi}_1^0 \rightarrow \tilde{\tau}_1 + \tau \\ \quad \quad \quad \downarrow \\ \quad \quad \quad \tau \ell^+ \ell^- \nu \end{array}$$

and the neutrinos from the successive  $\tau$  decays. However, we will not explicitly cut on  $\cancel{E}_T$  in the event selection in order to keep the analysis complementary to searches for  $R$ -parity conserving SUSY.

It should be kept in mind, that the discovery of a  $\cancel{E}_T$  signal does not necessarily contradict  $R_p$  models.  $\cancel{E}_T$  alone is not sufficient to distinguish  $R$ -parity violating from  $R$ -parity conserving SUSY. Further observables, like kinematic edges, will be needed to gain insights in the SUSY mass spectrum. Finally, a lepton (linear) collider may be needed to clarify the nature of the LSP and the source of the missing energy.

## V. DISCOVERY POTENTIAL AND MASS RECONSTRUCTION

### A. Cut Selection and Significances

We now employ in addition to the pre-selection cuts on reconstructed objects (see Sec. IV B) further cuts in order to increase the signal significance and the signal over background ratio. We show, that with an integrated luminosity of only  $200 \text{ pb}^{-1}$  at  $\sqrt{s} = 7$  TeV a discovery of the benchmark scenario BC1 is possible.

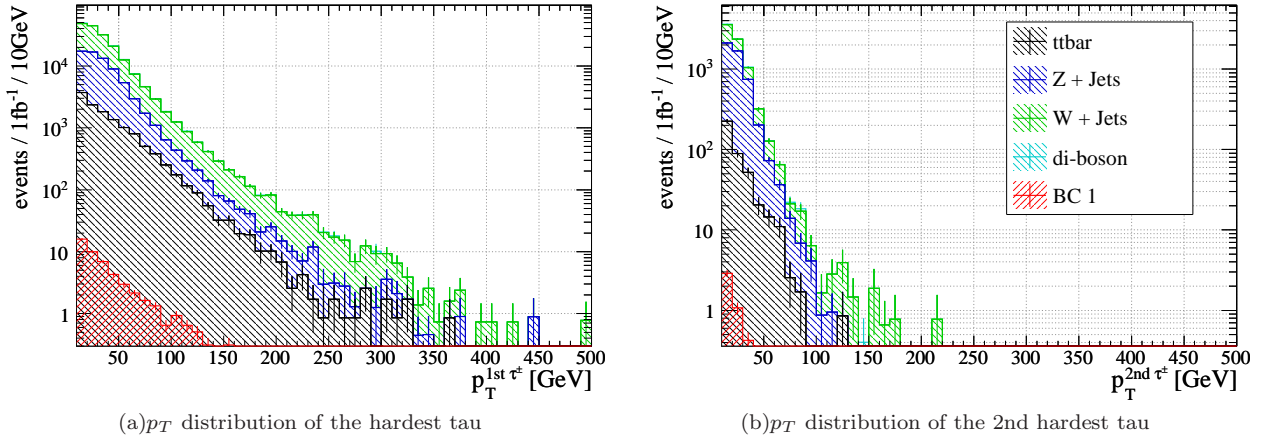


FIG. 8: (Visible)  $p_T$  distributions of the two hardest identified taus after object selection cuts and overlap removal.

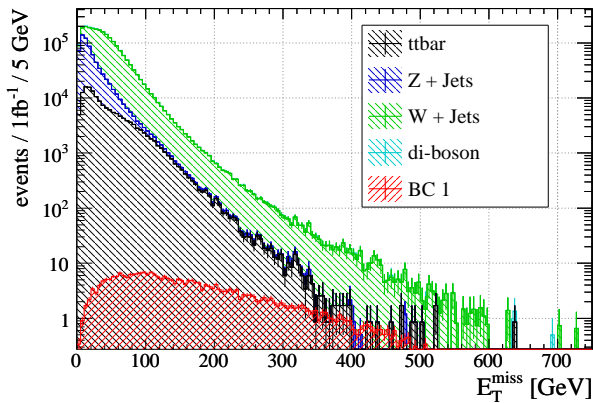


FIG. 9: Missing transverse energy,  $\cancel{E}_T$ , distribution after object selection cuts and overlap removal.

From the kinematic properties presented in Sec. IV C, we implement the following cuts:

- $p_T(1st \mu^\pm) > 40$  GeV. We demand at least one muon with  $p_T > 40$  GeV in the final state.
- $p_T(1st e^\pm) > 32$  GeV. We demand an electron with  $p_T > 32$  GeV in the final state.
- $p_T(2nd e^\pm) > 7$  GeV. We demand at least a second electron in each event. Note, that  $p_T > 7$  GeV corresponds to the electron pre-selection cut, *cf.* Tab. VI.
- $\sum p_T^\ell > 230$  GeV. We demand the  $p_T$  sum of all electrons and muons to be larger than 230 GeV.
- $HT' > 200/300/400$  GeV. We employ also different cuts on the  $p_T$  sum of the four hardest jets, namely 200 GeV, 300 GeV and 400 GeV, respectively.

The cut selection was optimized with the help of the TMVA toolkit [77]. The cuts were chosen so as

to improve the signal to background ratio, based on simulated annealing [78]. This was iterated with different sets of event selection variables, while some cuts were left fixed. We found that slightly different cuts increase the signal significance marginally for our Monte Carlo samples, but only at the cost of a higher risk to accept QCD events, which we could not simulate. Several other variables, like the  $\ell^+\ell^-$  invariant mass as  $Z$ -veto or the  $W$  transverse mass, were tested as well. However, they turned out to be of less relevance in combination with the variables finally used.

The cut flow is given in Tab. VII and visualized in Fig. 10. We also quote the signal to square root of background ratio,  $S/\sqrt{B}$  (second last column), and the significance  $Z_0$  [79] (last column) assuming a relative background uncertainty of 50%. For a definition of  $Z_0$  and related measures of significance see App. B.

We have chosen such a large systematic uncertainty for the SM backgrounds as a conservative approach, because uncertainties are expected from jet and lepton energy scales as well as the predictions of cross sections. The ATLAS collaboration for example estimates the systematic uncertainties for an integrated luminosity of  $1\text{fb}^{-1}$  to be 50% for the background from QCD multijet events and 20% for the background from  $t\bar{t}$ ,  $W$ +jets,  $Z$ +jets, and  $W$  pairs in the context of SUSY searches [60]. In our analysis we did not consider QCD multijet background explicitly. Additionally the systematic uncertainties will be larger for the very first searches and we therefore use the more conservative estimate of 50% uncertainty. The uncertainties in Tab. VII stem from the limited statistics of the simulated events (see Tab. V). Note that for  $W$ +jets we only show events with at least two jets at parton-level [58].

Employing only selection cuts (second row in Tab. VII), we observe that the number of SM background events (sixth column) is several orders of magnitude larger than the number of signal events (sev-

cut	$t\bar{t}$	Z+jets	W+jets	di-boson	all SM	BC 1	$S/\sqrt{B}$	$Z_0$
before cuts	155 500 $\pm$ 416	556 760 $\pm$ 681	1 505 250 $\pm$ 1127	40 720 $\pm$ 174	2 258 230 $\pm$ 1392	282.8 $\pm$ 2.8	0.2	-
$p_T(1st \mu^\pm) > 40$ GeV	16 745 $\pm$ 135	119 984 $\pm$ 313	180 009 $\pm$ 375	3 236 $\pm$ 49	319 975 $\pm$ 510	141.6 $\pm$ 2.0	0.3	-
$p_T(1st e^\pm) > 32$ GeV	1 492 $\pm$ 40	46.9 $\pm$ 5.9	102.4 $\pm$ 9.0	196.2 $\pm$ 12.7	1 837 $\pm$ 43	125.9 $\pm$ 1.9	2.9	-
$p_T(2nd e^\pm) > 7$ GeV	165.6 $\pm$ 14.4	2.2 $\pm$ 1.3	1.9 $\pm$ 1.3	15.2 $\pm$ 2.7	184.9 $\pm$ 14.8	113.7 $\pm$ 1.8	8.4	0.7
$\sum p_T^l > 230$ GeV	13.6 $\pm$ 4.2	$< 1.0$	1.0 $\pm$ 1.0	0.5 $\pm$ 0.5	15.1 $\pm$ 4.3	85.7 $\pm$ 1.6	22.0	4.9
$HT' > 200$ GeV	5.1 $\pm$ 2.1	$< 1.0$	1.0 $\pm$ 1.0	$< 1.0$	6.1 $\pm$ 2.3	60.3 $\pm$ 1.3	24.3	6.4
$HT' > 300$ GeV	3.4 $\pm$ 1.7	$< 1.0$	$< 1.0$	$< 1.0$	3.4 $\pm$ 1.7	56.6 $\pm$ 1.3	30.7	8.1
$HT' > 400$ GeV	$< 1.0$	$< 1.0$	$< 1.0$	$< 1.0$	$< 1.0$	52.6 $\pm$ 1.2	1.2	-

TABLE VII: Cut flow in BC1 at  $\sqrt{s} = 7$  TeV, scaled to an integrated luminosity of  $\int L dt = 1 \text{ fb}^{-1}$ . The uncertainties include statistical errors only. The significance  $Z_0$ , defined in App. B, assumes a background uncertainty of 50%.

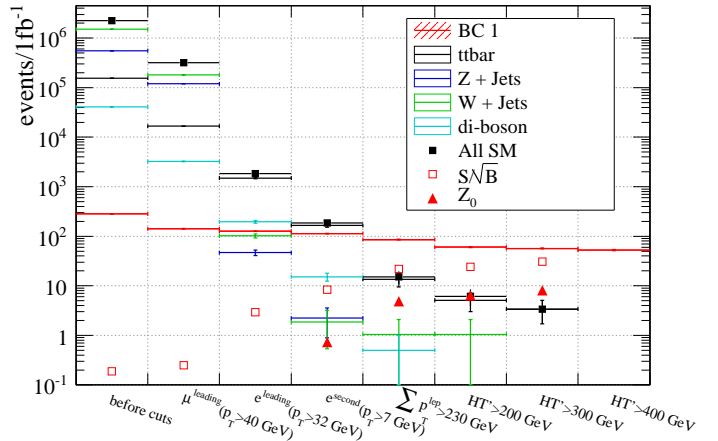


FIG. 10: Cut flow in BC1 at  $\sqrt{s} = 7$  TeV. As in Tab. VII, entries are scaled to an integrated luminosity of  $\int L dt = 1 \text{ fb}^{-1}$  and error bars include statistical uncertainties only. The significance  $Z_0$ , defined in App. B, assumes a background uncertainty of 50%.

enth column) [96]. Without any cuts, we expect at  $\sqrt{s} = 7$  TeV roughly 300 signal events for an integrated luminosity of  $1 \text{ fb}^{-1}$ .

We obtain a great improvement of the signal to background ratio to  $\mathcal{O}(0.1)$  by demanding one hard muon ( $p_T > 40$  GeV) and one hard electron ( $p_T > 32$  GeV) in the final state. At this stage the main backgrounds stem from leptonic decays of  $t\bar{t}$  (second column) and from leptonic decays of di-bosons (fifth column). These processes can produce an electron and muon at parton level. In addition, we also get some contributions from the  $W$ +jets and  $Z$ +jets backgrounds. Here, the second charged lepton of the first or second generation stems mainly from jets that are misidentified as a charged lepton. After the first two cuts, we already obtain a  $S/\sqrt{B}$  ratio of roughly three. However, if one takes into account systematic uncertainties, that are expected to be large at the early LHC run, one cannot observe a clear signal, *cf.* the last column in Tab. VII.

Demanding at least a second electron in the final state (fourth row) the situation further improves. We now have a signal to background ratio of roughly one and a  $S/\sqrt{B}$  ratio of 8.4. Therefore, by demanding two (hard enough) electrons and one muon in the final state, a signal of the scenario BC1 might already be visible in early LHC data, even though the significance  $Z_0$  is still small without further cuts.

As we have shown in Figs. 5 and 6, the electrons and muons of the signal events also have on average larger transverse momenta than the charged leptons from SM processes. We therefore demand in the sixth row in Tab. VII the  $p_T$  sum of the electrons and muons to be larger than 230 GeV; *cf.* Fig. 7. With this cut we obtain a number of signal events that is roughly six

times larger than the number of background events. A clear signal of BC1 should now be visible, because  $S/\sqrt{B} = 22$  and  $Z_0 = 4.9$ .

Up to now, we have only employed the electrons and muons that stem mainly from the stau LSP decays. However, in a typical SUSY event at the LHC, we will first produce a pair of strongly interacting sparticles. These sparticles then cascade decay down to the LSP producing hard jets in the final state. As can be seen in Fig. 3, these jets are in general harder than the jets from SM backgrounds. Therefore, we demand in Tab. VII as the last cut the  $p_T$  sum of the four hardest jets, Fig. 4, to be larger than 200 GeV (third last column), 300 GeV (second last column), or 400 GeV (last column), respectively. We show different cuts for  $HT'$  in order to show how the signal over background ratio improves with harder cuts on  $HT'$ .

For  $HT' > 200$  GeV, we already obtain a background sample without di-boson events (fifth row). Because we only have produced a finite number of background events (see Tab. V), we mark a background free sample by “ $\lesssim 1.0$ ”. If we harden the cut further to  $HT' > 300$  GeV, we also veto all  $Z$ +jets and  $W$  + jets events. Finally for  $HT' > 400$  GeV, we obtain even a background free sample! Note that at the same time, the number of signal events is only reduced by 30% ( $HT' > 200$  GeV), 34% ( $HT' > 300$  GeV) and 39% ( $HT' > 400$  GeV), respectively, compared to no cut on  $HT'$ .

We thus can further improve the significances  $S/\sqrt{B}$  and  $Z_0$  with a cut on  $HT'$ . For example, for  $HT' > 300$  GeV, we obtain  $S/\sqrt{B} = 24$  and  $Z_0 = 8.1$ . A signal is clearly visible. Note, that we cannot give meaningful numbers for the significances for  $HT' > 400$  GeV, because our background samples are not large enough. In addition, even if we cut away all the backgrounds in Tab. VII we still might have some small (unknown) QCD backgrounds. Therefore, we employ the  $HT' > 300$  GeV cut for our parameter scans in the next section in order to get meaningful results. It is the main purpose of the  $HT' > 400$  GeV cut to show that a (nearly) background free sample is possible.

We conclude, that the cuts presented in Tab. VII allow a discovery of the benchmark scenario BC1 with early LHC data. Scaling down the luminosity, we have found that even with an integrated luminosity of  $200 \text{ pb}^{-1}$  we still get  $Z_0 > 5$ ! We also want to point out that we only used electrons, muons and jets. Our analysis does thus not rely on the reconstruction and identification of missing energy,  $b$ -jets and taus, which might be more difficult with early data. In the next section we show, that the cuts work also quite well beyond BC1.

## B. Discovery Potential with early LHC Data

We now extend our previous analysis to a more extensive parameter region. We still restrict ourselves to early LHC data. We focus on regions of the  $B_3$  mSUGRA parameter space with different mass spectra compared to BC1 but with the same non-vanishing lepton number violating coupling, *i.e.*  $\lambda_{121} = 0.032$  at  $M_{\text{GUT}}$ . For that purpose we perform a two dimensional parameter scan in the  $M_{1/2}$ - $\tan\beta$  plane around BC1 ( $M_{1/2} = 400$  GeV,  $\tan\beta = 13$ ).

We have chosen a scan in  $M_{1/2}$  and  $\tan\beta$  for the following reasons. Due to the RGE running, every sparticle mass increases with increasing  $M_{1/2}$ , especially the masses of the strongly interacting sparticles [26, 29, 51], *cf.* Fig. 18(a) and Fig. 18(b). By varying  $M_{1/2}$  we can thus investigate the discovery potential as a function of the SUSY mass scale.

In contrast, changing  $\tan\beta$  does not affect most of the sparticle masses (see Fig. 18) and therefore also leaves the total sparticle production cross section unchanged. This can be seen in Fig. 11(a), where we present the total SUSY particle pair production cross section (at  $\sqrt{s} = 7$  TeV) as a function of  $M_{1/2}$  and  $\tan\beta$ . For example, increasing  $M_{1/2}$  from 320 GeV to 500 GeV reduces the cross section from 2 pb to 0.1 pb. Note that for  $M_{1/2} = 320$  GeV ( $M_{1/2} = 500$  GeV) we have squark masses mostly around 680 GeV (1 TeV) and a gluino mass of roughly 760 GeV (1.1 TeV); see Fig. 18(b) and Fig. 18(a), in App. A. But changing  $\tan\beta$  (for fixed  $M_{1/2}$ ) leaves the cross section almost unchanged.

However, increasing  $\tan\beta$  decreases the stau LSP mass, *cf.* Fig. 18(d). Increasing  $\tan\beta$  increases the tau Yukawa coupling and thus its (negative) contribution to the stau mass from RGE running [26, 29, 51]. Additionally, a larger value of  $\tan\beta$  leads normally to a larger mixing between the left- and right-handed stau [97]. This further reduces the mass of the stau LSP. Therefore, with the help of  $\tan\beta$  we can change the kinematics of the LSP decay products and also the momentum of the tau from the decay of the  $\tilde{\chi}_1^0$  into the stau (and a tau). Note that the mass of the  $\tilde{\chi}_1^0$  is nearly independent of  $\tan\beta$  (see Fig. 18(c)), because it is bino-like around BC1.

We show the results of the parameter scans in Fig. 11. The black region corresponds to excluded parameter points, with tachyons [3] or which violate the Higgs mass or stau mass bounds from LEP [98], *i.e.*  $m_{h^0} > 90$ –114.4 GeV [80, 81], depending on the SUSY parameters [99], and  $m_{\tilde{\tau}_1} > 86$  GeV [32]. We lowered the Higgs mass bound by 3 GeV to account for numerical uncertainties of SOFTSUSY [3, 82–84]. Note, that most of the parameter points in Fig. 11 are also consistent with the observed anomalous magnetic moment of the muon, with  $\text{BR}(b \rightarrow s\gamma)$  and with the upper bound on  $\text{BR}(B_s \rightarrow \mu^+\mu^-)$  [32].

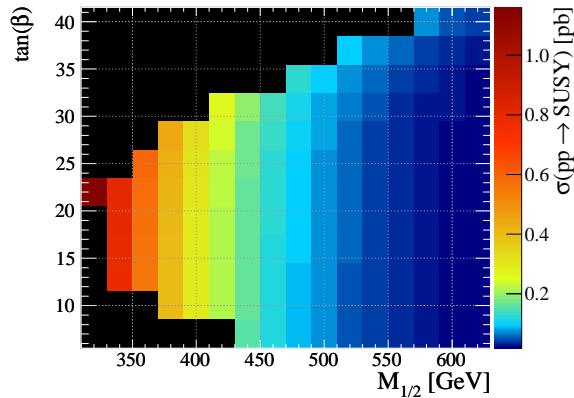
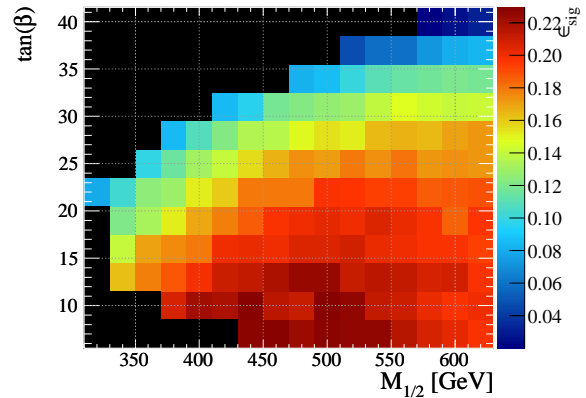
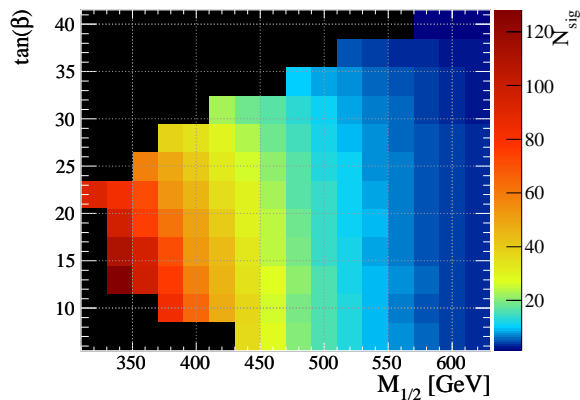
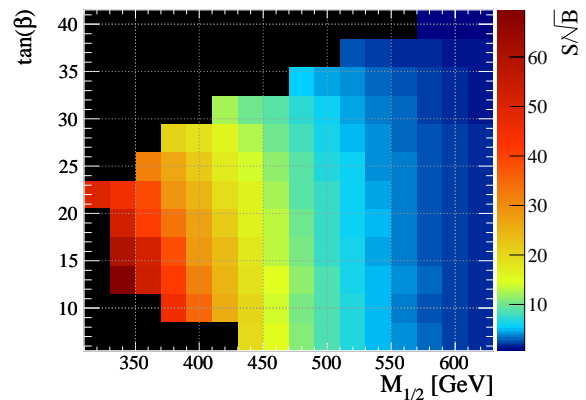
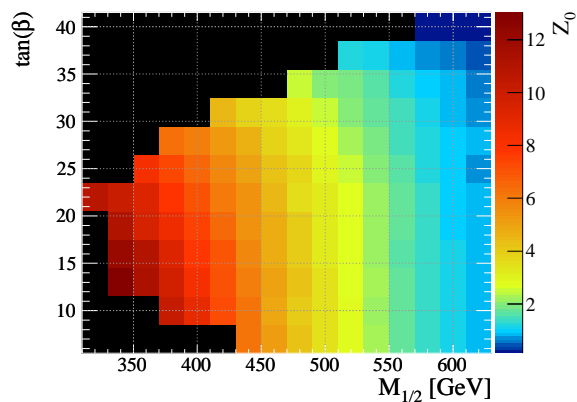
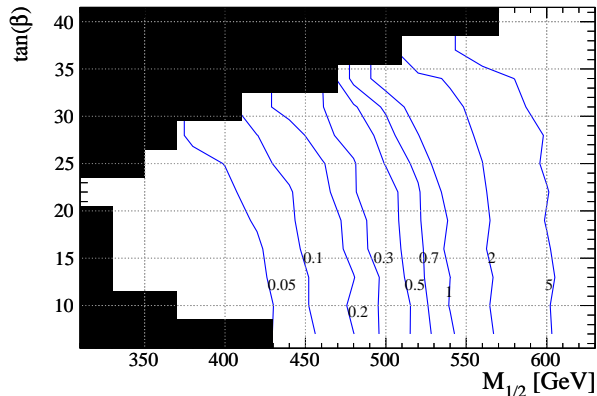
(a) Signal cross section in pb at LHC at  $\sqrt{s} = 7$  TeV.(b) Selection efficiency for the signal events at LHC at  $\sqrt{s} = 7$  TeV.(c) Number of selected signal events assuming an integrated luminosity of  $1 \text{ fb}^{-1}$  at  $\sqrt{s} = 7$  TeV.(d) Significance  $S/\sqrt{B}$  assuming an integrated luminosity of  $1 \text{ fb}^{-1}$  at  $\sqrt{s} = 7$  TeV.(e) Significance  $Z_0$  assuming an integrated luminosity of  $1 \text{ fb}^{-1}$  at  $\sqrt{s} = 7$  TeV.

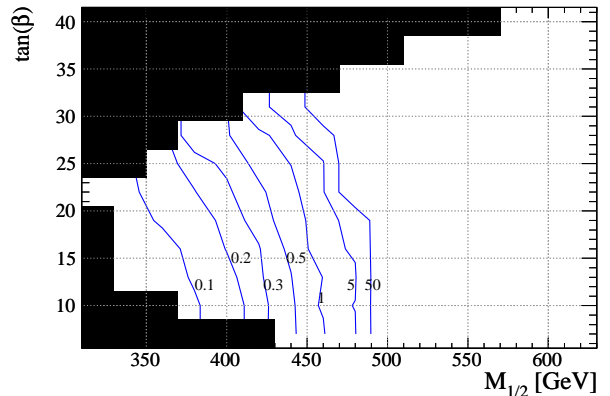
FIG. 11: Parameter scans in the  $M_{1/2}$ - $\tan(\beta)$  plane. The other mSUGRA parameters are those of BC1, *i.e.*  $M_0 = A_0 = 0$  GeV and  $\text{sgn}(\mu) = +1$ .  $Z_0$  is defined in App. B.

We present in Fig. 11(b) the selection efficiency for the signal events, *i.e.* the fraction of signal events that pass all the cuts in Tab. VII with  $HT' > 300$  GeV. For the scenario BC1 we obtain an efficiency of roughly 20%. Going beyond BC1, we can see in Fig. 11(b)

that the fraction of signal events that pass the cuts lies mostly between 10% and 23%. We conclude that the cuts work also quite well in other regions of the stau LSP parameter space than BC1.



(a) Estimated contours of minimum required integrated luminosity ( $\text{fb}^{-1}$ ) to reach  $S/\sqrt{B} > 5$



(b) Estimated contours of minimum required integrated luminosity ( $\text{fb}^{-1}$ ) to reach  $Z_0 > 5$  assuming a relative background uncertainty of 50%

FIG. 12: Minimum required integrated luminosity for a discovery at  $\sqrt{s} = 7$  TeV without [Fig. 12(a)] and with [Fig. 12(b)] systematic uncertainties included. The parameters are as in Fig. 11.

Fig. 11(b) also shows a correlation between the selection efficiency and  $\tan\beta$ : For fixed  $M_{1/2}$  the efficiency decreases if  $\tan\beta$  increases. This behavior can be easily understood. As mentioned above, increasing  $\tan\beta$  decreases the mass of the stau LSP. In this case, the decay products of a light stau LSP have on average smaller momenta compared to a heavy one. Therefore, less electrons and muons from stau LSP decays will pass the cuts in Tab. VII.

This also explains why we very often obtain a better selection efficiency for larger values of  $M_{1/2}$  (and fixed  $\tan\beta$ ). Increasing  $M_{1/2}$  increases the mass of all SUSY particles including the stau LSP. The SM particles from cascade decays and LSP decays have then on average larger momenta and thus pass the cuts more easily. However, when going to very large  $M_{1/2}$  the efficiency can again decrease, because the strongly interacting particles are very heavy and thus their decay products are highly boosted. The final state particles might then fail the isolation cuts.

By multiplying the signal cross section [Fig. 11(a)] with the signal efficiency [Fig. 11(b)], we obtain in Fig. 11(c) the number of signal events that pass the cuts for an integrated luminosity of  $1 \text{ fb}^{-1}$  at  $\sqrt{s} = 7$  TeV. For a light spectrum, *i.e.*  $M_{1/2} \lesssim 350$  GeV, we observe that 100 or more signal events pass the cuts. If we go to a heavier spectrum ( $M_{1/2} \gtrsim 500$  GeV), where the squarks and gluinos masses are  $\gtrsim 1$  TeV, we see that the number of signal events reduces to 20 or less. Although  $\mathcal{O}(10)$  signal events are enough to claim a discovery of new physics, we do not have enough events for a reconstruction of the sparticle masses, especially the stau LSP mass. We will address this issue in Sec. V C.

We finally present the resulting significances: In Fig. 11(d) we give  $S/\sqrt{B}$  as a naive estimator and

in Fig. 11(e)  $Z_0$  as a more realistic estimator. Note that  $Z_0$  is defined in App. B.

With an integrated luminosity of  $1 \text{ fb}^{-1}$  at  $\sqrt{s} = 7$  TeV,  $S/\sqrt{B}$  suggests that stau LSP scenarios up to  $M_{1/2} \lesssim 540$  GeV can be discovered. Note that  $M_{1/2} = 540$  GeV corresponds to squark masses [gluino masses] of 1.1 TeV [1.2 TeV]; see Fig. 18(b) [Fig. 18(a)], in App. A. If we include a 50% systematic uncertainty on the background estimate the discovery reach is reduced to  $M_{1/2} \lesssim 460$  GeV. In this case we have squark masses (gluino masses) around 950 GeV (1.1 TeV). We want to point out that due to the striking multi-lepton signature, the discovery reach for stau LSP scenarios with early LHC data is larger than that for  $R$ -parity conserving mSUGRA models [85].

We have also translated the significances of Fig. 11(d) and Fig. 11(e) to the minimum integrated luminosity that is required for a five sigma discovery. For  $S/\sqrt{B}$  this can easily be done, because  $S/\sqrt{B}$  scales with the square root of the luminosity. For  $Z_0$  the procedure is more involved, *cf.* App. B. The results for  $S/\sqrt{B}$  [ $Z_0$ ] are shown in Fig. 12(a) [Fig. 12(b)]. We can see in Fig. 12(b) that the benchmark scenario BC1 can be discovered with an integrated luminosity of less than  $200 \text{ pb}^{-1}$ . If the systematic uncertainties are under good control one might even claim a discovery with roughly  $50 \text{ pb}^{-1}$ , *cf.* Fig. 12(a).

### C. Stau Mass Estimate

We have shown in the last section that the stau LSP scenario with a non-vanishing  $\lambda_{121}$  coupling can already be tested quite stringently with early LHC data. If a discovery has been made, one would try to reconstruct the sparticle mass spectrum; especially the stau

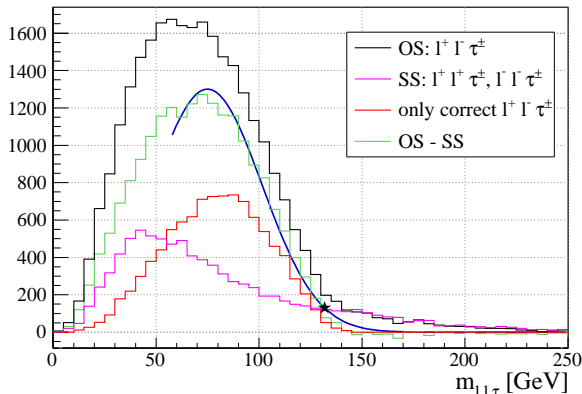


FIG. 13: Invariant mass distribution of the visible part of the hardest tau,  $\tau^\pm$ , with the two nearest (in  $\Delta R$ ) charged leptons,  $\ell$ , of the first or second generation. The black line (purple line) gives the distribution for the opposite-sign (same-sign) lepton pair,  $\ell^+\ell^-$  ( $\ell^\pm\ell^\mp$ ), plus the tau. The distribution is denoted by OS (SS). The green line shows the difference of the OS and SS distributions. The red histogram corresponds to the correct  $\tau^\pm\ell^+\ell^-$  combination, *i.e.* all three leptons stem from the same stau decay. We also fitted a Gaussian (blue line) to the green histogram.

LSP mass. We therefore propose a method to estimate the latter. Note, that we do not include systematic uncertainties. This has to be done after a discovery.

In and around BC1, the stau LSP decays via the 4-body mode

$$\tilde{\tau}_1^\pm \rightarrow \tau^\pm \ell^+ \ell^- \nu, \quad (7)$$

where  $\ell$  denotes an electron or muon; see Tab. II. By calculating the invariant mass of the stau LSP decay products one can in principle reconstruct its mass. But due to the initial neutrino and the neutrino in the subsequent tau decay, not all decay products are visible. However, we can still build the invariant mass of the  $\ell^+\ell^-$  pair with the visible part of the (hadronically decaying) tau. We then expect a kinematic endpoint in the invariant mass distribution, which should lie at the true stau LSP mass.

The black line in Fig. 13 shows the invariant mass distribution of the  $\ell^+\ell^-$  pair plus the visible part of the tau. The distribution corresponds to 50 000 BC1 signal events [100]. We do not include the SM backgrounds, because as shown in the previous section, it is possible to select a (nearly) background free data sample, *cf.* Tab. VII. Leptons are combined as follows. In each event we select the hardest identified tau. We then look for the two closest opposite sign (OS)  $\ell$ s in  $\Delta R = \sqrt{\Delta\phi^2 + \Delta\eta^2}$ . Finally, we calculate the invariant mass of these three leptons. If such a lepton triplet cannot be found in an event, we discard it for mass reconstruction. Note, that we do not employ a detector simulation here. We only employ the following cuts. Electrons and muons (hadronically decaying taus) are identified if their (visible)  $p_T$  is larger

than 7 GeV (10 GeV). The electrons and muons (tau decay products) must also lie within  $|\eta| < 2.5$ . We use the same setup in what follows if not otherwise mentioned. As an additional cut only those selected combinations are used, where the distance in  $\Delta R$  between both leptons and the tau is smaller than 1.5. In principle this cut may distort the invariant mass spectrum, especially for very high stau masses. We checked both options with and without this cut and observed, that both give nearly identical results in the precision of the estimated stau mass.

We see in Fig. 13 that the black line has a poorly defined endpoint at the true stau mass of 148 GeV. This is due to combinatorial backgrounds, *i.e.* we sometimes combine the wrong tau and electrons or muons with each other. Various other combination methods have also been studied, for example starting from the hardest electron or muon or using  $\Delta\phi$  instead of  $\Delta R$ . A small improvement is possible by vetoing the combination  $\tau\mu^+\mu^-$ . This does not increase the fraction of correct combinations but reduces the number of wrong combinations. The reason is, that the stau LSP can not decay to  $\tau\mu^+\mu^-\nu$  via a coupling  $\lambda_{121}$ ; *cf.* Tab. II. We did not veto the  $\tau\mu^+\mu^-$  combination as this keeps the method more model independent.

In 18% of all events no combination can be found, because no hadronic tau in the given kinematic range exists. In an independent 18% of all events there is only a tau, which does not stem from a stau decay, *i.e.* every method will choose the wrong tau. With our method, 30% of the chosen combinations are correct, while 25% include a (wrong) tau lepton that stems from the  $\tilde{\chi}_1^0$  decay, which belongs to the same decay chain as the chosen leptons. In 14% of the combinations the tau neither stems from a stau nor a  $\tilde{\chi}_1^0$  decay and in 15% at least one lepton stems from the other stau decay in the event. In 10% at least one lepton comes from another source, *i.e.* not from a stau decay.

In order to reduce the combinatorial backgrounds and thus to sharpen the kinematic endpoint of the invariant mass, we also combine the hardest tau with the nearest same sign (SS) lepton pair,  $\ell^\pm\ell^\pm$ . The respective invariant mass distribution is given by the purple line in Fig. 13. We then subtract the  $\tau$ +SS distribution (purple line) from the  $\tau$ +OS distribution (black line) and obtain the distribution given by the green line denoted by OS–SS.

The OS–SS invariant mass distribution now follows much closer the distribution that arises from the correct  $\tau\ell^+\ell^-$  triplet (red histogram in Fig. 13). Without the cut on the angular distance between the two leptons and the tau the same sign distribution shows a long tail at high invariant masses, which leads to an over-subtraction at high masses. This can be explained by the fact, that one of the same sign leptons mostly stems from the other stau decay in the event or another source and therefore often has a larger angle to the first lepton leading to higher invariant masses.



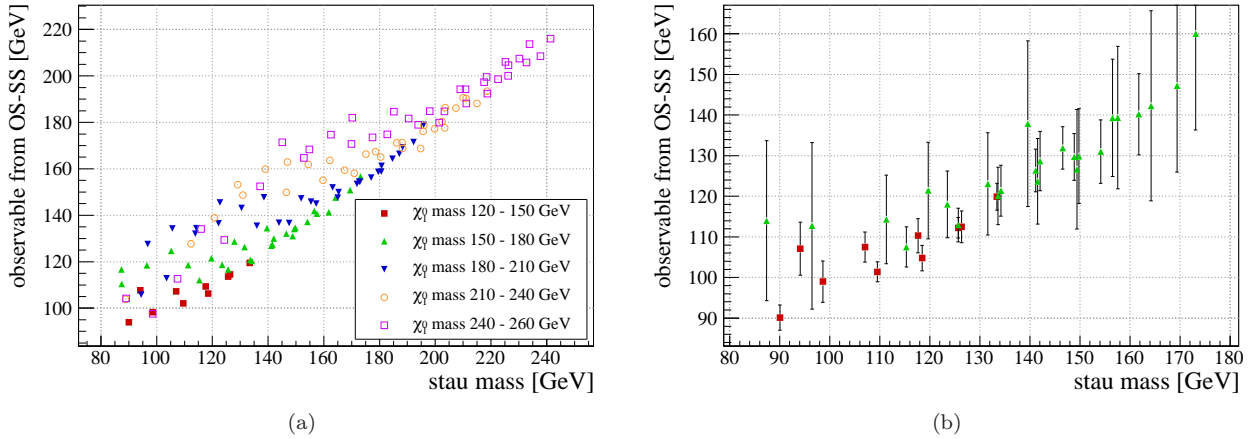


FIG. 14: Stau mass sensitive observable versus true stau mass (see text for definition) for the scenarios presented in Sec. VB. Different colors and shapes of the points correspond to different intervals of the  $\tilde{\chi}_1^0$  mass. Fig. 14(a): For each parameter point, 10 000 signal events were simulated. Fig. 14(b): Estimates for an integrated luminosity of  $5 \text{ fb}^{-1}$  including event selection cuts. Only scenarios where at least 150 events pass the cuts are used. The error bars show to what precision the estimated stau mass can be measured. The errors correspond to statistical fluctuations and are estimated as described in the text.

Still one can find stau mass sensitive observables, like the intersection of the OS–SS distribution with the  $x$ -axis, which show a good correlation with the true stau mass.

We observe that the OS–SS histogram has an endpoint near the true endpoint. As the stau mass sensitive observable, we fit a Gaussian on the OS–SS distribution and take the value, where it drops to 10% of its maximum (marked by a star in Fig. 13) [101]. Although the observable lies below the *true* stau mass of 148 GeV, we can estimate it from the observable as long as there is a clear and known correlation between the two. This has successfully been demonstrated for example in Ref. [56, 86].

This is indeed the case as one can see in Fig. 14(a). Here we take the stau LSP scenarios of our parameter scans in Sec. VB. We then simulated 10 000 signal events for each scenario and determined from these the estimated stau mass as described above. The different colors of the points in Fig. 14(a) correspond to different  $\tilde{\chi}_1^0$  masses.

We can see in Fig. 14(a) a clear correlation between the true stau LSP mass and the observable from the OS–SS invariant mass distribution. We also see that there is only a small systematic dependence of the estimated mass on the  $\tilde{\chi}_1^0$  mass. For example, for a stau mass of 120 GeV, the observable can increase roughly from 100 GeV to 140 GeV, if the  $\tilde{\chi}_1^0$  mass increases from 120 GeV to 240 GeV. This is because a heavier  $\tilde{\chi}_1^0$  leads to a harder tau from the  $\tilde{\chi}_1^0 \rightarrow \tilde{\tau}_1 \tau$  decay.

One can use Fig. 14(a) to translate the observable to the true stau mass. Such an analysis is even possible in a limited way with early LHC data, as can be seen in Fig. 14(b), where we again show the observable versus the true stau mass. Now, we have only

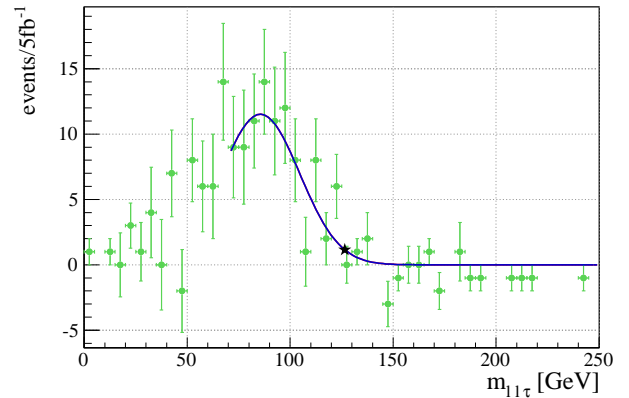


FIG. 15: OS–SS distribution as in Fig. 13, but here including event selection cuts and randomly selecting events corresponding to an integrated luminosity of  $5 \text{ fb}^{-1}$ , *i.e.* uncertainties and fluctuations correspond to those expected for  $5 \text{ fb}^{-1}$ .

included scenarios, where at least 150 events in  $5 \text{ fb}^{-1}$  pass our cuts. Otherwise, we would not have enough statistics for the mass reconstruction. We applied the event selection cuts that are given in Tab. VII with  $HT' > 300 \text{ GeV}$ . The error bars correspond to the precision with which the observable can be measured assuming an integrated luminosity of  $5 \text{ fb}^{-1}$ . We do not include systematic uncertainties.

The statistical uncertainties in Fig. 14(b) were estimated in the following way. Out of 10 000 simulated signal events, events have been randomly chosen to get a sub-sample corresponding to an integrated luminosity of  $5 \text{ fb}^{-1}$ . This procedure was repeated 100 times for each point to obtain different sub-samples.

The observable of these sub-samples follows a Gaussian distribution, where its width corresponds to the statistical uncertainties in Fig. 14(b). Fig. 15 shows an example of one sub-sample for the BC1 scenario.

We can see that with an integrated luminosity of  $5 \text{ fb}^{-1}$ , rough estimates of the stau LSP mass are possible.

## VI. TAU IDENTIFICATION

We have seen in Sec. V C that the identification (ID) of tau leptons is vital for the mass reconstruction of the stau LSP. However, as we have pointed out already in the discussion of Fig. 2(d), tau ID within the framework of BC1 is difficult. We now give a short explanation for this observation.

The ID of hadronic decays of tau leptons in the detector makes use of special properties of the hadronic tau decay. First one expects one or three charged pion tracks, *i.e.* *single-prong* and *three-prong* events, respectively. Furthermore, jets from tau decays are usually rather collimated compared to jets from the hadronization of quarks or gluons. The ratio of energy deposits in the electromagnetic calorimeter to those in the hadronic calorimeter can give further hints. Leptonic tau decays ( $\tau \rightarrow \nu_e \nu_\tau e$  and  $\tau \rightarrow \nu_\mu \nu_\tau \mu$ ) are usually not considered, because the decay length of tau leptons is mostly too small to distinguish the decay products from prompt electrons or muons.

However, the special event topologies in BC1 (and possibly other beyond-the-SM models) can make it very difficult to reliably identify tau decays in those events. In BC1, and also more generally in nearly all stau LSP scenarios, a very dense environment is expected, *i.e.* a high multiplicity of charged particles; see Tab. II. Therefore, overlaps between the tau jets and jets from the SUSY decay chain or leptons from the stau LSP decay are very likely. In addition, different tau jets might also overlap. A reduced tau ID efficiency compared to most SM processes is thus expected.

Both *Delphes* [50] and *PGS* [76] use approaches for the detector simulation of tau leptons, which can be seen as simplified versions of algorithms for tau lepton ID used by the experiments. Observables, like electromagnetic collimation and track isolation, are calculated from the simulated calorimeter deposits and tracks. Cuts are then applied to decide, whether a jet is tagged as a tau lepton. In both codes we only consider 1-prong candidates, *i.e.* candidates with one assigned track.

We show in Fig. 17 the efficiency for the ID of hadronic tau decays in BC1 and for (SM)  $Z \rightarrow \tau\tau + 1\text{jet}$  production. We also give the fraction of wrongly tagged tau jets per event. We show results for the fast detector simulation *Delphes* [Fig. 17(a)-Fig. 17(d)] as

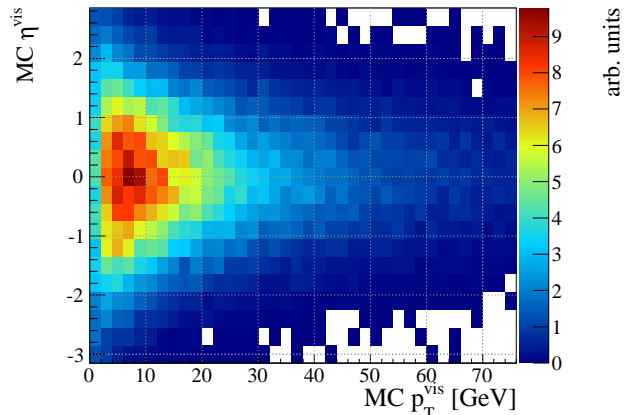


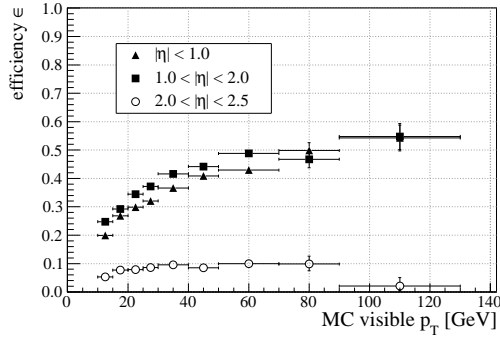
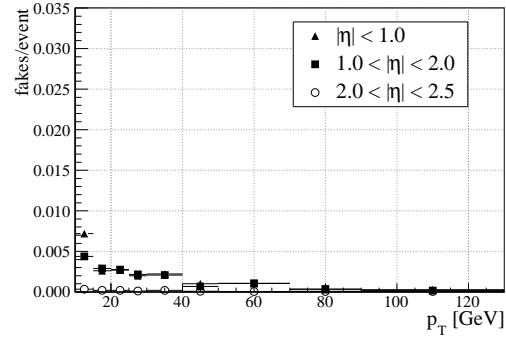
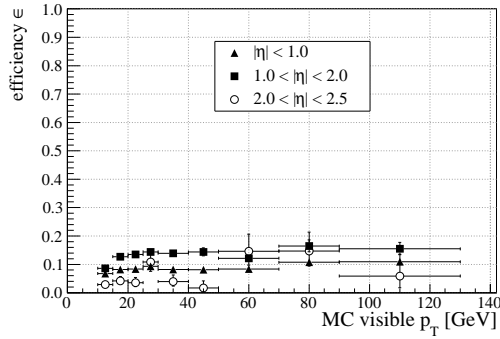
FIG. 16: Number of hadronically decaying taus in the  $\eta$ - $p_T$  plane in arbitrary units. Only the visible parts of the taus are considered. No detector simulation and acceptance cuts have been applied. Bins without entries are white.

well as for *PGS* [Fig. 17(e)-Fig. 17(h)]. In addition, the standard overlap removal is applied [102].

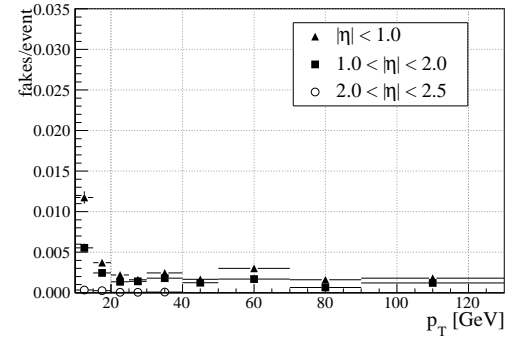
Both detector simulations show that the ID efficiency is significantly lower in BC1 than in  $Z \rightarrow \tau\tau + 1\text{jet}$ . This has to be kept in mind, as many methods used in the experiments to estimate the tau ID efficiency rely on  $Z \rightarrow \tau\tau$  as a “standard candle” [56]. For example, for a (visible) tau- $p_T$  of 45 GeV in the inner part of the detector, the tau ID efficiency is 40% [60%] for  $Z \rightarrow \tau\tau$  but only 10% [30%] in BC1 according to *Delphes* [*PGS*], *cf.* Fig. 17(a) and Fig. 17(c) [Fig. 17(e) and Fig. 17(g)] at the respective working points on the efficiency-vs-rejection curve.

We also see in Fig. 17 that in general the tau ID in *Delphes* has a much lower fake rate than the one in *PGS*. However this comes at the cost of a slightly worse identification efficiency giving a different working point of the tau ID. As a conservative approach, we take the numbers from *Delphes*. Even in the optimistic case the tau ID efficiency cannot be expected to be better than about 25% over a wide  $p_T$  range and can be even lower in the interesting low  $p_T$  range, *i.e.* (visible) tau- $p_T \lesssim 30$  GeV. One can see in Fig. 16, that most tau leptons even have visible transverse momenta below our ID threshold of 10 GeV. Given that only 65% of all tau leptons decay hadronically the efficiency with respect to all tau leptons is below 10%. This means for less than one in 10000 BC1 events, one can expect all four tau leptons to be correctly tagged as such. This explains the low tau multiplicity of Fig. 2(d).

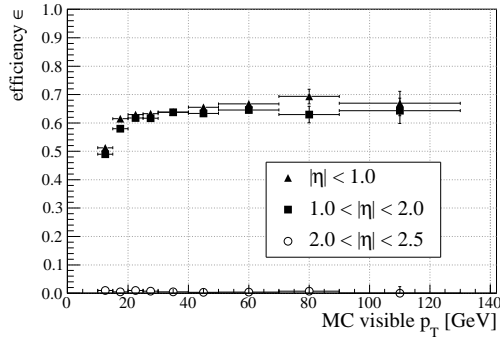
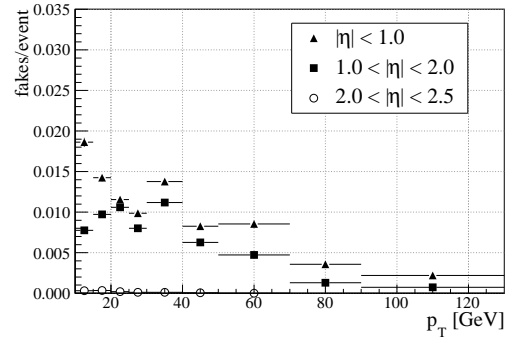
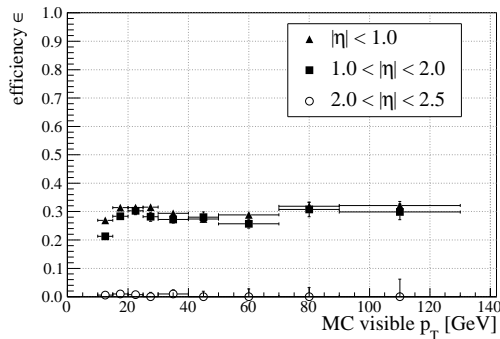
In conclusion the identification of hadronic tau decays in BC1 and presumably in similar models as well, is challenging for the experiments at the LHC. Precise estimates of the identification efficiency need studies with full-fledged detector simulations. The direct estimate of the efficiency from measured data may be

(a) ID efficiency in  $Z \rightarrow \tau\tau + 1\text{jet}$  for Delphes(b) Fake rate in  $Z \rightarrow \tau\tau + 1\text{jet}$  for Delphes

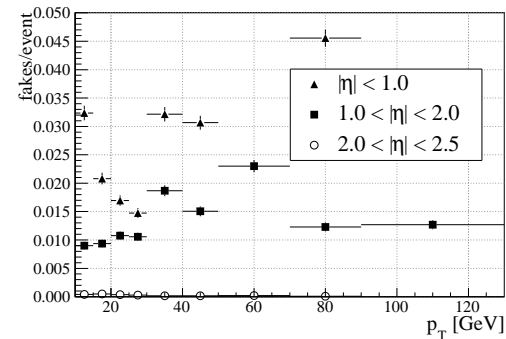
(c) ID efficiency in BC 1 for Delphes



(d) Fake rate in BC 1 for Delphes

(e) ID efficiency in  $Z \rightarrow \tau\tau + 1\text{jet}$  for PGS(f) Fake rate in  $Z \rightarrow \tau\tau + 1\text{jet}$  for PGS

(g) ID efficiency in BC 1 for PGS



(h) Fake rate in BC 1 for PGS

FIG. 17: Tau ID efficiencies and fake rates in BC 1 and  $Z \rightarrow \tau\tau + 1\text{jet}$  for PGS and Delphes.

difficult as the numbers are expected to differ strongly between BC1 events and the usual “standard candles”, like  $Z \rightarrow \tau\tau$ .

## VII. SUMMARY AND CONCLUSION

If  $R$ -parity is violated, the lightest supersymmetric particle (LSP) is unstable. Therefore, it can be charged and any supersymmetric particle can be the LSP. Within the framework of minimal supergravity (mSUGRA), this allows for a large region of the parameter space, where the scalar tau (stau) and not the lightest neutralino is the LSP.

We have investigated the LHC phenomenology of  $R$ -parity violating mSUGRA with a stau LSP and with lepton number violation. In this model, one non-vanishing  $R$ -parity violating operator is present at the grand unification scale in addition to the  $R$ -parity conserving mSUGRA parameters. Focusing on pair production of strongly interacting SUSY particles, we classified in Sec. III all possible LHC signatures at parton level; *cf.* Tabs. II-IV for an overview. The most promising scenarios for the early LHC are those where the stau LSP decays via a non-vanishing  $\lambda_{121}$  (or  $\lambda_{212}$ ) coupling. This is because each stau LSP decays purely leptonically via a 4-body decay into two electrons or muons, a tau and a neutrino; *cf.* Tab. II.

We have here performed a first comprehensive signal over background analysis of stau LSP scenarios at the LHC with early data. We employed pair production of all SUSY particles as our signal. Our results using fast simulations of the ATLAS detector show, that the LHC has a good potential to test  $R$ -parity violating supersymmetry with a stau LSP and multi-lepton final states already in the next two years. The benchmark scenario BC1 (see Tab. I) with the 4-body decay  $\tilde{\tau}_1^\pm \rightarrow \tau^\pm \ell^+ \ell^- \nu$  has many electrons and muons in its final states. This allows the selection of a (nearly) background-free sample of  $\mathcal{O}(50)$  BC1 events using an integrated luminosity of  $1 \text{ fb}^{-1}$  at  $\sqrt{s} = 7 \text{ TeV}$ .

In our event selection used to derive the discovery potential we avoid using tau-leptons. Naively one would expect large numbers of tau leptons in the final states from the decay  $\tilde{\chi}_1^0 \rightarrow \tilde{\tau}_1 + \tau$  and the LSP decay. However, the reconstruction and identification efficiency for the tau leptons is expected to be very low, *i.e.* not larger than 25% (see Sect. VII), because of their small momenta. But a precise estimate is only possible with a full detector simulation. Additionally, overlaps between jets from tau decay products and other jets and leptons in the event further reduce the efficiency by a factor 2-3 compared to simple event topologies, like  $Z \rightarrow \tau^+ \tau^-$ . Our estimates using fast detector simulations predict no identified tau leptons in the majority of the BC1 events, even though four tau leptons are expected at tree level. Instead, we only use the transverse momenta of the leading and sub-

leading electron and the leading muon, the scalar sum of the electron and muon transverse momenta,  $\sum p_T^\ell$  and the visible hadronic mass,  $HT' = \sum_{\text{jet } 1-4} p_T$ .

In wide ranges of the  $M_{1/2}$ - $\tan\beta$  parameter space around the benchmark point one can achieve event selection efficiencies of about 20% for nearly background-free samples. Including a systematic uncertainty of 50% on the background estimate the discovery reach is up to  $M_{1/2} = 460 \text{ GeV}$  for  $1 \text{ fb}^{-1}$ . The benchmark scenario BC1 itself can even be discovered with an integrated luminosity of less than  $200 \text{ pb}^{-1}$ .

Despite being potentially easy to discover in the first LHC data, there are some difficulties in measuring the mass of the stau-LSP in BC1. Due to large combinatorial backgrounds, the selection of correct combinations of stau-decay products is difficult and sometimes even impossible, because the visible momenta of the tau leptons are too small to be reconstructed. Neutrinos from the stau decay and the successive tau decay only allow for the reconstruction of a smooth endpoint in the invariant mass distribution. However, we could show that observables can be reconstructed, which show a good correlation with the true stau mass, even though they will need much more data than  $5 \text{ fb}^{-1}$  to provide a precise measurement.

## Acknowledgments

We thank John Conway and Kyoungchul Kong for helpful discussions. S.G. thanks the Alexander von Humboldt Foundation for financial support. The work of S.G. was also partly financed by the DOE grant DE-FG02-04ER41286. S.F. thanks the Bonn-Cologne Graduate School of Physics and Astronomy for financial support. The work of H.D. was supported by the BMBF “Verbundprojekt HEP–Theorie” under the contract 05H09PDE and the Helmholtz Alliance “Physics at the Terascale”. The work of K.D., S.F. and P.W. was supported by the German Federal Ministry of Education and Research (BMBF) under the contract 05H09PDA.

## Appendix A: Properties of the benchmark scenario BC1

We review in this appendix some properties of the benchmark scenarios BC1 as described in Ref. [32].

### 1. Branching Ratios and Mass Spectrum

In Tab. VIII we show the supersymmetric mass spectrum and the branching ratios (BRs) in the BC1 scenario. The non-vanishing  $B_3$  coupling at  $M_{\text{GUT}}$  is  $\lambda_{121}|_{\text{GUT}} = 0.032$ . The other mSUGRA parameters

mass [GeV]	channel	BR	channel	BR	
$\tilde{\tau}_1^-$	148	$\mu^+ e^- \tau^- \bar{\nu}_e$	$e^+ e^- \tau^- \bar{\nu}_\mu$	<b>32.2%</b>	<b>32.1%</b>
		$\mu^- e^+ \tau^- \nu_e$	$e^- e^+ \tau^- \nu_e$	<b>17.9%</b>	<b>17.8%</b>
$\tilde{e}_R^-$	161	$e^- \nu_\mu$	$\mu^- \nu_e$	<b>50%</b>	<b>50%</b>
$\tilde{\mu}_R^-$	161	$\tilde{\tau}_1^+ \mu^- \tau^-$	$\tilde{\tau}_1^- \mu^- \tau^+$	51.2%	48.7%
$\tilde{\chi}_1^0$	162	$\tilde{\tau}_1^+ \tau^-$	$\tilde{\tau}_1^- \tau^+$	49.8%	49.8%
$\tilde{\nu}_\tau$	261	$\tilde{\chi}_1^0 \nu_\tau$	$W^+ \tilde{\tau}_1^-$	67.2%	32.8%
$\tilde{\nu}_e (\tilde{\nu}_\mu)$	262	$\tilde{\chi}_1^0 \nu_e (\nu_\mu)$	$e^- \mu^+ (e^+)$	92.4%	<b>7.5%</b>
$\tilde{e}_L^- (\tilde{\mu}_L^-)$	274	$\tilde{\chi}_1^0 e^- (\mu^-)$	$e^- \bar{\nu}_e (\bar{\nu}_\mu)$	91.9%	<b>8.1%</b>
$\tilde{\tau}_2^-$	278	$\tilde{\chi}_1^0 \tau^-$	$\tilde{\tau}_1^- Z$	63.0%	17.6%
		$h \tilde{\tau}_1^-$		19.4%	
$\tilde{\chi}_2^0$	303	$\tilde{\nu}_\tau \bar{\nu}_\tau$	$\tilde{\nu}_\tau^* \nu_\tau$	9.1%	9.1%
		$\tilde{\tau}_1^- \tau^+$	$\tilde{\tau}_1^+ \tau^-$	9.1%	9.1%
		$\tilde{\nu}_e \bar{\nu}_e$	$\tilde{\nu}_e^* \nu_e$	8.5%	8.5%
		$\tilde{\nu}_\mu \bar{\nu}_\mu$	$\tilde{\nu}_\mu^* \nu_\mu$	8.5%	8.5%
		$\tilde{e}_L^- e^+$	$\tilde{e}_L^+ e^-$	4.5%	4.5%
		$\tilde{\mu}_L^- \mu^+$	$\tilde{\mu}_L^+ \mu^-$	4.5%	4.5%
		$\tilde{\tau}_2^- \tau^+$	$\tilde{\tau}_2^+ \tau^-$	3.1%	3.1%
		$\tilde{\chi}_1^0 h$		3.5%	
		$\tilde{\chi}_1^-$	303	$\tilde{\nu}_\tau \tau^-$	$\tilde{\nu}_\mu \mu^-$
		$\tilde{\nu}_e e^-$	$\tilde{\tau}_1^- \bar{\nu}_\tau$	18.6%	16.7%
		$\tilde{e}_L^- \bar{\nu}_e$	$\tilde{\mu}_L^- \bar{\nu}_\mu$	8.1%	8.1%
		$\tilde{\tau}_2^- \bar{\nu}_\tau$	$\tilde{\chi}_1^0 W^-$	5.5%	4.0%
$\tilde{\chi}_3^0$	514	$\tilde{\chi}_1^- W^+$	$\tilde{\chi}_1^+ W^-$	28.9%	28.9%
		$\tilde{\chi}_2^0 Z$	$\tilde{\chi}_1^0 Z$	24.1%	10.2%
		$\tilde{\chi}_1^0 h$	$\tilde{\tau}_1^- \tau^+$	1.8%	1.0%
		$\tilde{\tau}_1^+ \tau^-$		1.0%	
$\tilde{\chi}_4^0$	529	$\tilde{\chi}_1^- W^+$	$\tilde{\chi}_1^+ W^-$	26.5%	26.5%
		$\tilde{\chi}_2^0 h$	$\tilde{\chi}_1^0 h$	17.5%	7.1%
		$\tilde{\nu}_\tau \bar{\nu}_\tau$	$\tilde{\nu}_\tau^* \nu_\tau$	1.8%	1.8%
		$\tilde{\nu}_e \bar{\nu}_e$	$\tilde{\nu}_e^* \nu_e$	1.8%	1.8%
		$\tilde{\nu}_\mu \bar{\nu}_\mu$	$\tilde{\nu}_\mu^* \nu_\mu$	1.8%	1.8%
		$\tilde{\tau}_2^- \tau^+$	$\tilde{\tau}_2^+ \tau^-$	1.7%	1.7%
		$\tilde{\chi}_1^0 Z$	$\tilde{\chi}_2^0 Z$	1.8%	1.4%

mass [GeV]	channel	BR	channel	BR	
$\tilde{\chi}_2^-$	532	$\tilde{\chi}_2^0 W^-$	$\tilde{\chi}_1^- Z$	28.3%	25.3%
		$\tilde{\chi}_1^- h$	$\tilde{\chi}_1^0 W^-$	19.8%	8.1%
		$\tilde{\tau}_2^- \bar{\nu}_\tau$	$\tilde{e}_L^- \bar{\nu}_e$	4.4%	3.7%
		$\tilde{\mu}_L^- \bar{\nu}_\mu$	$\tilde{\nu}_\tau^* \tau^-$	3.7%	2.8%
		$\tilde{\nu}_e^* e^-$	$\tilde{\nu}_\mu^* \mu^-$	1.6%	1.6%
$t_1$	647	$\tilde{\chi}_1^+ b$	$\tilde{\chi}_1^0 t$	44.0%	23.7%
		$\tilde{\chi}_2^+ b$	$\tilde{\chi}_2^0 t$	17.0%	15.4%
$b_1$	780	$\tilde{\chi}_1^- t$	$\tilde{\chi}_2^- t$	36.0%	25.2%
		$\tilde{\chi}_2^0 b$	$W^- \tilde{t}_1$	22.0%	12.0%
		$\tilde{\chi}_1^0 b$	$\tilde{\chi}_3^0 b$	2.4%	1.2%
$b_2$	816	$\tilde{\chi}_2^- t$	$\tilde{t}_1 W^-$	40.8%	15.2%
		$\tilde{\chi}_1^0 b$	$\tilde{\chi}_1^- t$	12.7%	10.0%
		$\tilde{\chi}_2^0 b$	$\tilde{\chi}_3^0 b$	8.6%	6.7%
		$\tilde{\chi}_2^+ b$		6.0%	
$\tilde{d}_R (\tilde{s}_R)$	820	$\tilde{\chi}_1^0 d(s)$		99.4%	
$\tilde{u}_R (\tilde{c}_R)$	822	$\tilde{\chi}_1^0 u(c)$		99.4%	
$t_2$	835	$\tilde{\chi}_4^0 t$	$\tilde{\chi}_1^+ b$	23.5%	23.0%
		$\tilde{\chi}_2^+ b$	$\tilde{t}_1 Z$	15.0%	12.3%
		$\tilde{\chi}_3^0 t$	$\tilde{\chi}_2^0 t$	9.6%	9.6%
		$\tilde{t}_1 h$	$\tilde{\chi}_1^0 t$	5.7%	2.3%
$\tilde{u}_L (\tilde{c}_L)$	852	$\tilde{\chi}_1^- d(s)$	$\tilde{\chi}_2^0 u(c)$	64.6%	31.8%
		$\tilde{\chi}_2^+ d(s)$	$\tilde{\chi}_4^0 u(c)$	1.5%	1.1%
		$\tilde{\chi}_1^0 u(c)$		1.0%	
$d_L (\tilde{s}_L)$	855	$\tilde{\chi}_1^- u(c)$	$\tilde{\chi}_2^0 d(s)$	61.6%	31.8%
		$\tilde{\chi}_2^- u(c)$	$\tilde{\chi}_1^0 d(s)$	3.8%	1.8%
		$\tilde{\chi}_4^0 d(s)$		1.4%	
$\tilde{g}$	932	$\tilde{q}\tilde{q}$	$\tilde{q}^* q$	25.0%	25.0%
		$\tilde{t}_1 \tilde{t}$	$\tilde{t}_1^* t$	9.5%	9.5%
		$\tilde{b}_1 \tilde{b}$	$\tilde{b}_1^* b$	7.7%	7.7%
		$\tilde{b}_2 \tilde{b}$	$\tilde{b}_2^* b$	5.2%	5.2%

TABLE VIII: SUSY mass spectrum and BRs of the benchmark scenario BC1 [32]. Only decays with a BR of at least 1% are shown.  $R$ -parity violating decays are in bold face.

are  $M_0 = A_0 = 0$  GeV,  $M_{1/2} = 400$  GeV,  $\tan\beta = 10$ , and  $\text{sgn}(\mu) = +1$ .

The heavy part of the spectrum, *e.g.* gluinos and squarks, looks very similar to mSUGRA scenarios with a  $\tilde{\chi}_1^0$  LSP, like SPS1a [87]. In BC1, these sparticles mainly decay via two-body decays mediated by the usual  $R$ -parity conserving gauge interactions into a lighter sparticle and a quark.

Also the middle part of the mass spectrum, *i.e.* in Tab. VIII masses of roughly 300 – 500 GeV, is very similar to many  $\tilde{\chi}_1^0$  LSP mSUGRA scenarios. This includes most of the charginos and neutralinos. The heaviest neutralinos,  $\tilde{\chi}_3^0$  and  $\tilde{\chi}_4^0$ , and the heaviest chargino,  $\tilde{\chi}_2^+$ , are Higgsino-like whereas the  $\tilde{\chi}_2^0$  and  $\tilde{\chi}_1^+$  are wino-like. These sparticles also mainly decay via two-body decays involving gauge interactions.

However, the light part of the spectrum in Tab. VIII looks very different than the  $R$ -parity conserving mSUGRA scenarios with a  $\tilde{\chi}_1^0$  LSP. We now have a stau LSP and the  $\tilde{\chi}_1^0$  is only the next-to-next-to-next-to LSP (NNNLSP). However, it is nearly degenerate in

mass with the slightly lighter right-handed selectron,  $\tilde{e}_R$  and smuon,  $\tilde{\mu}_R$ .

We also observe that some of the lighter sparticles decay via  $R$ -parity violating interactions, with BRs larger than 1%. The stau LSP that can only decay via a  $R$ -parity violating operator. Because it does not directly couple to the dominant  $L_1 L_2 \bar{E}_1$ -operator, it decays in BC1 via a four-body decay, *cf.* Tab. II. The  $\tilde{e}_R$  decays mainly via  $R$ -parity violating interactions. This is because it couples directly via  $\lambda_{121}$  and can thus decay via a two-body decay into two nearly massless SM particles. The competing  $R$ -parity conserving decay mode is a three-body decay, namely  $\tilde{e}_R^- \rightarrow \tilde{\tau}_1^\pm \tau^\mp e^-$ . The  $\tilde{\chi}_1^0$  NNNLSP is also unstable. It decays mainly into a tau plus the stau LSP. See Refs. [32, 49] for further details.

## 2. Masses and Mass Differences

We review in Fig. 18 some sparticle masses and mass differences in the  $M_{1/2}$ - $\tan\beta$  plane. The scan is cen-

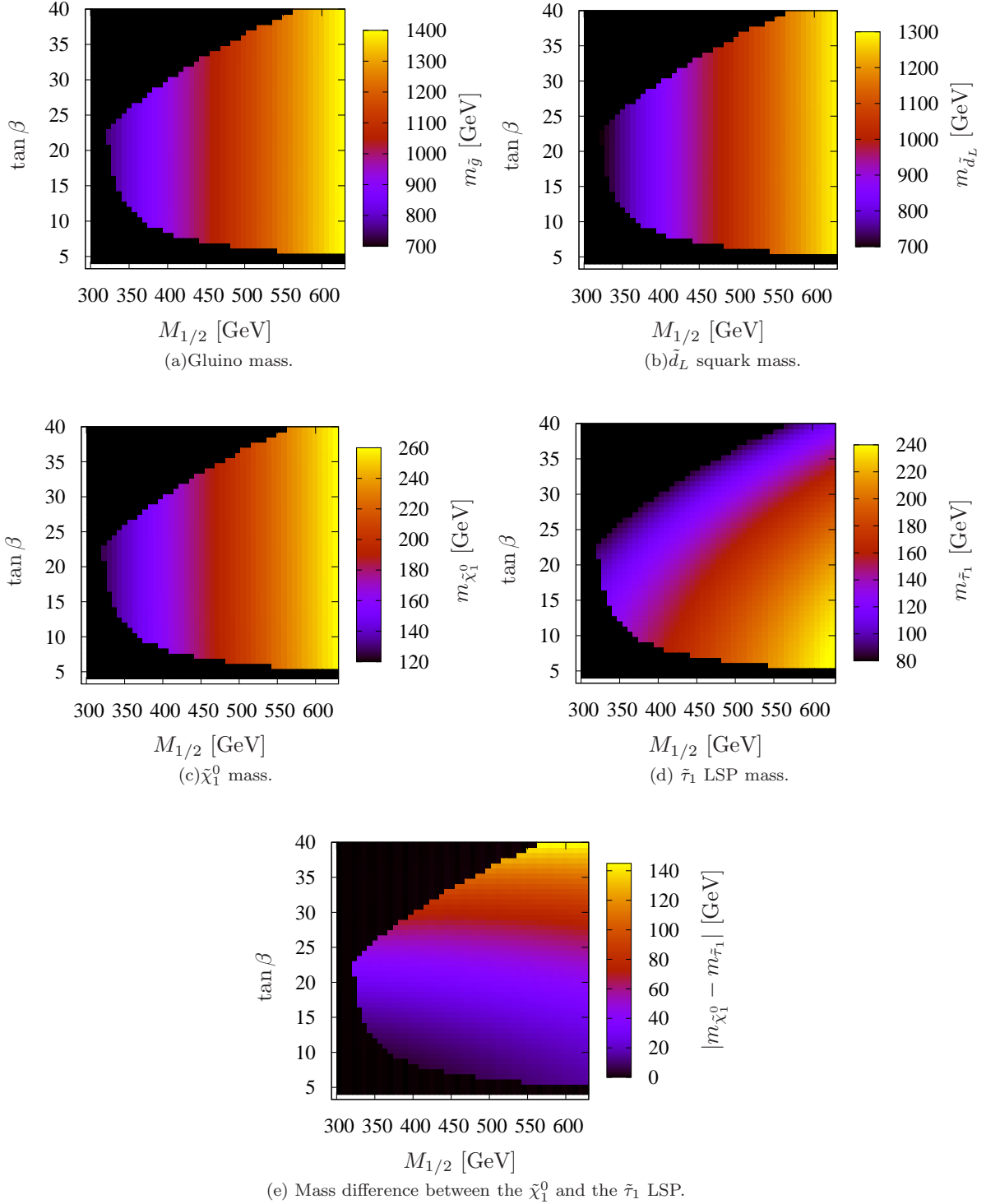


FIG. 18: Masses and mass differences in the  $M_{1/2}$ - $\tan\beta$  plane. The other mSUGRA parameter are that of BC1, *i.e.*  $M_0 = A_0 = 0$  GeV and  $\text{sgn}(\mu) = +1$ . The blackened out region is excluded due to tachyons or the LEP Higgs or  $\tilde{\tau}_1$  mass bounds; see also Sec. VB. The complete parameter space shown in the figures posses a stau LSP.

tered around BC1 ( $M_{1/2} = 400$  GeV and  $\tan\beta = 13$ ) and corresponds to the parameter space for which we investigated the discovery potential with early LHC data, *i.e.* Figs. 11 and 12.

We show in Figs. 18(a), 18(b), and 18(c) the mass of the gluino, the left-handed down-type squark,  $\tilde{d}_L$ , and the  $\tilde{\chi}_1^0$ , respectively. We observe that these masses depend in first approximation only on  $M_{1/2}$ : they in-

crease with increasing  $M_{1/2}$ ; see Refs. [51, 88] for further details.

However, the stau LSP mass, Fig. 18(d), is different. It also depends strongly on  $\tan\beta$ . For increasing  $\tan\beta$  the stau LSP mass decreases. As already described in Sec. VB, this is mainly due to the following effects. On the one hand,  $\tan\beta$  increases the tau Yukawa coupling and thus its negative contribution to the RGE running of the stau masses. On the other hand, a larger value of  $\tan\beta$  leads in general to a larger mixing between the left-handed and right-handed stau. This than results in one lighter stau mass eigenstate; *cf. e.g.* Ref. [27].

Therefore, we can change the mass difference between the  $\tilde{\chi}_1^0$  and the stau LSP by changing  $\tan\beta$  as visualized in Fig. 18(e).

## Appendix B: Significance Definitions

The expected signal significance for a given set of event selection cuts depends on the significance definition used and the estimated systematic uncertainties. In many phenomenological publications the simple  $S/\sqrt{B}$  ratio is used, whereas more detailed experimental analyses use other definitions. We compare some definitions in Tab. IX, which make different assumptions on the underlying statistical properties and give a very short review of those. For details we refer to Refs. [79, 89].

In all cases the  $p$ -value of a given number of observed events under the background-only hypothesis with a certain number of expected background events is related to the significance  $Z$  by

$$p = \int_Z^\infty \frac{1}{\sqrt{2\pi}} e^{-x^2/2} dx = 1 - \Phi(Z), \quad (\text{B1})$$

where  $\Phi$  is the cumulative distribution of the standard Gaussian.

In all cases we use the so-called Asimov dataset, *i.e.* we estimate the expected number of signal ( $S$ ) and background ( $B$ ) events by our Monte Carlo estimate and the expected number of observed events by  $n_{\text{obs}} = S + B$ . Assuming Poisson statistics the  $p$ -value of observing  $n_{\text{obs}}$  events when  $B$  background events are expected is

$$p_{\text{P}} = \sum_{n=n_{\text{obs}}}^{\infty} P_{\text{P}}(n; B) = \sum_{n=n_{\text{obs}}}^{\infty} \frac{B^n}{n!} e^{-B}, \quad (\text{B2})$$

where  $P_{\text{P}}$  is the Poisson distribution. Using Wilks' theorem the corresponding significance  $Z_{\text{P}} = \Phi^{-1}(1 - p_{\text{P}})$  can be approximated as

$$Z_{\text{W}} = \sqrt{2(S+B) \ln(1+S/B) - 2S} \quad (\text{B3})$$

in the limit of large statistics. In our case this approximation is very good and  $Z_{\text{W}}$  and  $Z_{\text{P}}$  have nearly

identical values.  $Z_{\text{W}}$  itself can be approximated with the simple  $S/\sqrt{B}$  in the limit of  $S \ll B$  by expanding the logarithm. This approximation is clearly not valid for our nearly background free sample and is the reason for the discrepancy between  $S/\sqrt{B}$  and  $Z_{\text{P}}$  in Tab. IX.

The significance is reduced by uncertainties on the background estimate. As the background is estimated from Monte Carlo itself, limited statistics of the background Monte Carlo translates into uncertainties on the estimate of  $B$ , which are not included in the previous definitions of significance. The ratio between Monte Carlo and data luminosity  $\tau = \frac{L^{\text{MC}}}{L^{\text{data}}}$  is used to relate the  $m$  Monte Carlo background events passing the cuts to the background estimate  $b = m/\tau$ . The probability to observe  $n = S + B$  events is therefore

$$\begin{aligned} P(n, m; S+B, \tau B) &= P_{\text{P}}(n; S+B) \cdot P_{\text{P}}(m; \tau B) \\ &= P_{\text{P}}(n+m; S+B+\tau B) \\ &\quad \cdot P_{\text{Bi}}(n|n+m; \rho), \end{aligned} \quad (\text{B4})$$

with  $\rho = \frac{S+B}{S+B+\tau B}$  and  $P_{\text{Bi}}$  denoting the binomial distribution. One can test the background only hypothesis ( $S=0$ ) with a standard frequentist binomial parameter test, giving the  $p$ -value

$$p_{\text{Bi}} = \sum_{j=n}^{n+m} P_{\text{Bi}}(j|n+m; 1/(1+\tau)). \quad (\text{B5})$$

The estimated uncertainty of estimating the true  $b\tau$  by  $m$  is  $\sqrt{m}$ , which gives the correspondence  $\sigma_b = \sqrt{m}/\tau$  and with the estimate of  $b$  finally  $\tau = b/\sigma_b^2$ . This relationship can be used to provide an ad-hoc background uncertainty  $\sigma_b$  to the Binomial  $p$ -value, *cf.* Eq. (B5). We used this method in our definition of  $Z_0$  to set a fixed relative background uncertainty of  $f = 50\%$ , *i.e.* in summary

$$\tau' = 1/(b \cdot f^2) \quad (\text{B6})$$

$$n'_{\text{off}} = b \cdot \tau' \quad (\text{B7})$$

$$n'_{\text{on}} = s + b \quad (\text{B8})$$

$$p_0 = \sum_{k=n'_{\text{on}}}^{n'_{\text{on}}+n'_{\text{off}}} P_{\text{Bi}}(k|n'_{\text{off}}+n'_{\text{on}}; 1/(1+\tau')) \quad (\text{B9})$$

$$Z_0 = \Phi^{-1}(1 - p_0) \quad (\text{B10})$$

For large number of background events, as in our sample before cuts, this can lead to  $p_0 > 0.5$ , *i.e.* the significance is not well-defined anymore.

Finally we used a profile likelihood method to incorporate the uncertainty on the Monte Carlo estimate of the background in the significance. This has the advantage with respect to  $Z_{\text{Bi}}$ , that different scale factors  $\tau_i$  for different sub-samples  $i$  of the background can be treated correctly. A description of the method can be found in the documentation of the `SigCalc` code [89], that was used for the calculation of  $Z_{\text{PLH}}$ .

cut	all SM		BC1		$S/\sqrt{B}$	$Z_0$	$Z_{PLH}$	$Z_P$	$Z_{Bi}$
before cuts	2 258 230	$\pm$ 1392	282.8	$\pm$ 2.8	0.2	–	0.1	0.2	0.1
$p_T(1st \mu^\pm) > 40$ GeV	319 975	$\pm$ 510	141.6	$\pm$ 2.0	0.3	–	0.2	0.2	0.2
$p_T(1st e^\pm) > 32$ GeV	1 837	$\pm$ 43	125.9	$\pm$ 1.9	2.9	–	2.1	2.9	2.1
$p_T(2nd e^\pm) > 7$ GeV	184.9	$\pm$ 14.8	113.7	$\pm$ 1.8	8.4	0.7	5.5	7.6	5.5
$\sum p_T^\ell > 230$ GeV	15.1	$\pm$ 4.3	85.7	$\pm$ 1.6	22.0	4.9	8.8	14.5	8.8
$HT' > 200$ GeV	6.1	$\pm$ 2.3	60.3	$\pm$ 1.3	24.3	6.4	7.8	13.9	7.8
$HT' > 300$ GeV	3.4	$\pm$ 1.7	56.6	$\pm$ 1.3	30.7	8.1	7.9	15.2	8.1
$HT' > 400$ GeV	$\lesssim$ 1.0		52.6	$\pm$ 1.2					

TABLE IX: Cut flow and different significance definitions for BC1. We assumed an integrated luminosity of  $\int L = 1\text{fb}^{-1}$  at  $\sqrt{s} = 7$  TeV. The given uncertainties include statistical errors only. The significance  $Z_0$  includes a systematic uncertainty of 50%. For the first three rows  $Z_0$  is not well-defined.

- [1] R. Hempfling, Nucl. Phys. B **478** (1996) 3 [arXiv:hep-ph/9511288].
- [2] M. A. Diaz, J. C. Romao and J. W. F. Valle, Nucl. Phys. B **524** (1998) 23 [arXiv:hep-ph/9706315].
- [3] B. C. Allanach, A. Dedes and H. K. Dreiner, Phys. Rev. D **69** (2004) 115002 [Erratum-ibid. D **72** (2005) 079902] [arXiv:hep-ph/0309196].
- [4] H. K. Dreiner, C. Luhn and M. Thormeier, Phys. Rev. D **73** (2006) 075007 [arXiv:hep-ph/0512163]; H. K. Dreiner, C. Luhn, H. Murayama and M. Thormeier, Nucl. Phys. B **774** (2007) 127 [arXiv:hep-ph/0610026].
- [5] H. S. Lee, arXiv:1007.1040 [hep-ph].
- [6] H. P. Nilles, Phys. Rept. **110** (1984) 1.
- [7] S. P. Martin, In \*Kane, G.L. (ed.): Perspectives on supersymmetry\* 1-98. [hep-ph/9709356].
- [8] B. C. Allanach and C. H. Kom, JHEP **0804** (2008) 081 [arXiv:0712.0852 [hep-ph]].
- [9] H. K. Dreiner, S. Grab and M. Hanussek, arXiv:1005.3309 [hep-ph].
- [10] H. K. Dreiner, J. Soo Kim and M. Thormeier, arXiv:0711.4315 [hep-ph].
- [11] P. Minkowski, Phys. Lett. B **67** (1977) 421; R. N. Mohapatra and G. Senjanovic, Phys. Rev. Lett. **44** (1980) 912.
- [12] R. Barbier *et al.*, Phys. Rept. **420** (2005) 1 [arXiv:hep-ph/0406039].
- [13] E. J. Chun and H. B. Kim, Phys. Rev. D **60** (1999) 095006 [arXiv:hep-ph/9906392].
- [14] K. Choi, E. J. Chun and K. Hwang, Phys. Rev. D **64** (2001) 033006 [arXiv:hep-ph/0101026].
- [15] H. B. Kim and J. E. Kim, Phys. Lett. B **527** (2002) 18 [arXiv:hep-ph/0108101].
- [16] E. J. Chun and H. B. Kim, JHEP **0610** (2006) 082 [arXiv:hep-ph/0607076].
- [17] L. Covi and J. E. Kim, New J. Phys. **11** (2009) 105003 [arXiv:0902.0769 [astro-ph.CO]].
- [18] S. Bobrovskiy, W. Buchmuller, J. Hajer and J. Schmidt, arXiv:1007.5007 [hep-ph].
- [19] W. Buchmuller, L. Covi, K. Hamaguchi, A. Ibarra and T. Yanagida, JHEP **0703** (2007) 037 [arXiv:hep-ph/0702184].
- [20] H. -S. Lee, C. Luhn, K. T. Matchev, JHEP **0807** (2008) 065. [arXiv:0712.3505 [hep-ph]].
- [21] H. -S. Lee, K. T. Matchev, T. T. Wang, Phys. Rev. **D77** (2008) 015016. [arXiv:0709.0763 [hep-ph]].
- [22] C. C. Jean-Louis and G. Moreau, arXiv:0911.3640 [hep-ph].
- [23] J. R. Ellis, J. S. Hagelin, D. V. Nanopoulos, K. A. Olive and M. Srednicki, Nucl. Phys. B **238** (1984) 453.
- [24] H. K. Dreiner, arXiv:hep-ph/9707435.
- [25] H. K. Dreiner and G. G. Ross, Nucl. Phys. B **365** (1991) 597.
- [26] M. A. Bernhardt, S. P. Das, H. K. Dreiner and S. Grab, Phys. Rev. D **79** (2009) 035003 [arXiv:0810.3423 [hep-ph]].
- [27] H. K. Dreiner, S. Grab and M. K. Trenkel, Phys. Rev. D **79** (2009) 016002 [Erratum-ibid. **79** (2009) 019902] [arXiv:0808.3079 [hep-ph]].
- [28] H. K. Dreiner, S. Grab, M. Krämer and M. K. Trenkel, Phys. Rev. D **75** (2007) 035003 [arXiv:hep-ph/0611195].
- [29] H. K. Dreiner and S. Grab, Phys. Lett. B **679** (2009) 45 [arXiv:0811.0200 [hep-ph]].
- [30] H. K. Dreiner and S. Grab, AIP Conf. Proc. **1200** (2010) 358 [arXiv:0909.5407 [hep-ph]].
- [31] G. F. Giudice and R. Rattazzi, Phys. Rept. **322** (1999) 419 [arXiv:hep-ph/9801271].
- [32] B. C. Allanach, M. A. Bernhardt, H. K. Dreiner, C. H. Kom and P. Richardson, Phys. Rev. D **75** (2007) 035002 [arXiv:hep-ph/0609263].
- [33] L. E. Ibanez and G. G. Ross, Phys. Lett. B **110** (1982) 215.
- [34] V. D. Barger, M. S. Berger, R. J. N. Phillips and T. Woehrmann, Phys. Rev. D **53** (1996) 6407 [arXiv:hep-ph/9511473]; H. K. Dreiner and H. Pois, arXiv:hep-ph/9511444.
- [35] B. C. Allanach, A. Dedes, H. K. Dreiner, Phys. Rev. **D60** (1999) 056002. [hep-ph/9902251].
- [36] B. de Carlos, P. L. White, Phys. Rev. **D54** (1996) 3427-3446. [hep-ph/9602381].
- [37] A. G. Akeroyd, M. A. Diaz, J. Ferrandis, M. A. Garcia-Jareno and J. W. F. Valle, Nucl. Phys. B **529** (1998) 3 [arXiv:hep-ph/9707395].
- [38] A. de Gouvea, A. Friedland and H. Murayama, Phys. Rev. D **59** (1999) 095008 [arXiv:hep-ph/9803481].
- [39] A. G. Akeroyd, C. Liu and J. H. Song, Phys. Rev. D **65** (2002) 015008 [arXiv:hep-ph/0107218].
- [40] A. Bartl, M. Hirsch, T. Kernreiter, W. Porod



- and J. W. F. Valle, JHEP **0311** (2003) 005 [arXiv:hep-ph/0306071].
- [41] M. A. Bernhardt, H. K. Dreiner, S. Grab and P. Richardson, Phys. Rev. D **78** (2008) 015016 [arXiv:0802.1482 [hep-ph]].
- [42] K. Ghosh, S. Mukhopadhyay and B. Mukhopadhyaya, arXiv:1007.4012 [hep-ph].
- [43] B. Mukhopadhyaya and S. Mukhopadhyay, arXiv:1005.3051 [hep-ph].
- [44] F. de Campos, O. J. P. Eboli, M. B. Magro, W. Porod, D. Restrepo, M. Hirsch and J. W. F. Valle, JHEP **0805** (2008) 048 [arXiv:0712.2156 [hep-ph]].
- [45] G. Abbiendi *et al.* [OPAL Collaboration], Eur. Phys. J. C **33** (2004) 149 [arXiv:hep-ex/0310054].
- [46] A. Heister *et al.* [ALEPH Collaboration], Eur. Phys. J. C **31** (2003) 1 [arXiv:hep-ex/0210014].
- [47] J. Abdallah *et al.* [DELPHI Collaboration], Eur. Phys. J. C **36** (2004) 1 [Eur. Phys. J. C **37** (2004) 129] [arXiv:hep-ex/0406009].
- [48] M. Hirsch, W. Porod, J. C. Romao and J. W. F. Valle, Phys. Rev. D **66** (2002) 095006 [arXiv:hep-ph/0207334].
- [49] B. C. Allanach, M. A. Bernhardt, H. K. Dreiner, S. Grab, C. H. Kom and P. Richardson, arXiv:0710.2034 [hep-ph].
- [50] S. Ovin, X. Rouby and V. Lemaître, arXiv:0903.2225 [hep-ph].
- [51] M. Drees and S. P. Martin, arXiv:hep-ph/9504324.
- [52] J. M. Butterworth, J. R. Ellis, A. R. Raklev and G. P. Salam, arXiv:0906.0728 [hep-ph].
- [53] J. M. Butterworth, B. E. Cox and J. R. Forshaw, Phys. Rev. D **65** (2002) 096014 [arXiv:hep-ph/0201098].
- [54] J. M. Butterworth, J. R. Ellis and A. R. Raklev, JHEP **0705** (2007) 033 [arXiv:hep-ph/0702150].
- [55] J. M. Butterworth, A. R. Davison, M. Rubin and G. P. Salam, Phys. Rev. Lett. **100** (2008) 242001 [arXiv:0802.2470 [hep-ph]].
- [56] G. Aad *et al.* [The ATLAS Collaboration], arXiv:0901.0512 [hep-ex].
- [57] G. P. Salam, arXiv:0906.1833 [hep-ph].
- [58] We have checked that  $W$  production in association with one jets at parton level plays no role after our cuts in Tab. VII have been applied.
- [59] T. Binoth, G. Ossola, C. G. Papadopoulos and R. Pittau, JHEP **0806** (2008) 082 [arXiv:0804.0350 [hep-ph]].
- [60] The ATLAS Collaboration, CERN-OPEN-2008-020, [arXiv:0901.0512 [hep-ex]].
- [61] B. C. Allanach, Comput. Phys. Commun. **143** (2002) 305 [arXiv:hep-ph/0104145].
- [62] B. C. Allanach and M. A. Bernhardt, Comput. Phys. Commun. **181** (2010) 232 [arXiv:0903.1805 [hep-ph]].
- [63] F. E. Paige, S. D. Protopopescu, H. Baer and X. Tata, arXiv:hep-ph/0312045.
- [64] G. Corcella *et al.*, JHEP **0101** (2001) 010 [arXiv:hep-ph/0011363].
- [65] G. Corcella *et al.*, arXiv:hep-ph/0210213.
- [66] S. Moretti, K. Odagiri, P. Richardson, M. H. Seymour and B. R. Webber, JHEP **0204** (2002) 028 [arXiv:hep-ph/0204123].
- [67] The version of Herwig used in this analysis was written by Peter Richardson and is available on request.
- [68] J. M. Butterworth, J. R. Forshaw and M. H. Seymour, Z. Phys. C **72** (1996) 637 [arXiv:hep-ph/9601371].
- [69] S. Frixione and B. R. Webber, JHEP **0206** (2002) 029 [arXiv:hep-ph/0204244].
- [70] S. Frixione, P. Nason and B. R. Webber, JHEP **0308** (2003) 007 [arXiv:hep-ph/0305252].
- [71] F. Caravaglios, M. L. Mangano, M. Moretti and R. Pittau, Nucl. Phys. B **539** (1999) 215 [arXiv:hep-ph/9807570].
- [72] M. L. Mangano, M. Moretti and R. Pittau, Nucl. Phys. B **632** (2002) 343 [arXiv:hep-ph/0108069].
- [73] M. L. Mangano, M. Moretti, F. Piccinini, R. Pittau and A. D. Polosa, JHEP **0307** (2003) 001 [arXiv:hep-ph/0206293].
- [74] J. Pumplin, D. R. Stump, J. Huston, H. L. Lai, P. Nadolsky, W. K. Tung, JHEP **0207** (2002) 012 [arXiv:hep-ph/0201195].
- [75] G. P. Salam and G. Soyez, JHEP **0705** (2007) 086 [arXiv:0704.0292 [hep-ph]].
- [76] J. Conway *et al.*, <http://www.physics.ucdavis.edu/~conway/research/software/pgs/pgs4-general.htm>
- [77] A. Hoecker *et al.*, arXiv:physics/0703039.
- [78] N. Metropolis, *et al.*, J. Chem. Phys. **21** (1953) 1087.
- [79] R. D. Cousins, J. T. Linnemann and J. Tucker, NIM A **595** (2008) 480–501.
- [80] S. Schael *et al.* [ALEPH Collaboration and DELPHI Collaboration and L3 Collaboration], Eur. Phys. J. C **47** (2006) 547 [arXiv:hep-ex/0602042].
- [81] R. Barate *et al.* [LEP Working Group for Higgs boson searches and ALEPH Collaboration and and], Phys. Lett. B **565** (2003) 61 [arXiv:hep-ex/0306033].
- [82] B. C. Allanach, S. Kraml and W. Porod, JHEP **0303** (2003) 016 [arXiv:hep-ph/0302102].
- [83] G. Degrassi, S. Heinemeyer, W. Hollik, P. Slavich and G. Weiglein, Eur. Phys. J. C **28** (2003) 133 [arXiv:hep-ph/0212020].
- [84] B. C. Allanach, A. Djouadi, J. L. Kneur, W. Porod and P. Slavich, JHEP **0409** (2004) 044 [arXiv:hep-ph/0406166].
- [85] H. Baer, V. Barger, A. Lessa and X. Tata, arXiv:1004.3594 [hep-ph].
- [86] T. Nattermann, K. Desch, P. Wienemann and C. Zendler, JHEP **0904** (2009) 057 [arXiv:0903.0714 [hep-ph]].
- [87] B. C. Allanach *et al.*, in *Proc. of the APS/DPF/DPB Summer Study on the Future of Particle Physics (Snowmass 2001)* ed. N. Graf, Eur. Phys. J. C **25** (2002) 113 [arXiv:hep-ph/0202233].
- [88] L. E. Ibanez, C. Lopez and C. Munoz, Nucl. Phys. B **256** (1985) 218.
- [89] G. Cowan, <http://www.pp.rhul.ac.uk/~cowan/stat/SigCalc/> (2008).
- [90] If the lifetime of the neutralino LSP is much larger than the age of the universe, it is still a good dark matter candidate. However, the trilinear  $R$ -parity violating couplings need in this case to be smaller than  $\mathcal{O}(10^{-20})$  [12]. Note that such  $R$ -parity violating scenarios are indistinguishable from  $R$ -parity conserving scenarios at colliders, because the neutralino LSP can escape detection.
- [91] Another early paper is Ref.[38], however, here  $R$ -parity is conserved.
- [92] For completeness, we give in this section also the signatures for a non-vanishing  $\bar{U}_i \bar{D}_j \bar{D}_k$  operator, where  $\bar{U}_i$  denotes an up-type quark  $SU(2)$  singlet super-

- field. Note that  $\bar{U}_i \bar{D}_j \bar{D}_k$  violates  $B_3$ ; *cf.* for example Ref. [3].
- [93] In principle, there can be additional stau LSP decays via  $R$ -parity violating couplings which are generated via RGE running. This is particularly important if the  $R$ -parity violating operator at the unification scale leads to a 4-body decay, whereas the generated one allows a 2-body decay; see Ref. [27] for a detailed discussion and for explicit examples. For the benchmark point BC1, for example,  $\lambda_{323}$  can be generated out of  $\lambda_{121}$  allowing a 2-body stau LSP decay, *i.e.*  $\tilde{\tau}_1^+ \rightarrow \mu^+ \bar{\nu}_\tau$ . However, this decay plays no significant role in this work, although it might be important in other regions of the parameter space. For the parameter scan in Sect. VB, the 2-body decay branching ratio is always  $< 1\%$  ( $\lesssim 10\%$ ) for  $\tan\beta < 25$  ( $\tan\beta > 25$ ).
- [94] In principle, tri-boson production can also contribute to the SM background. However, the production cross section is much smaller than the di-boson cross-section [59]. In addition, we expect that the cut on  $HT' = \sum_{\text{jet } 1-4} p_T$ , *i.e.* on the scalar sum of the transverse momenta of the four hardest jets, would veto nearly all tri-boson events that pass the lepton cuts, like the di-boson backgrounds; *cf.* Tab. VII.
- [95] We changed the default ATLAS settings in Delphes, as follows. The preselection cuts were adjusted according to Tab. VI. Furthermore we chose as the jet algorithm SIScone [75] with a cone radius of 0.4. The calculation of the missing transverse energy  $\cancel{E}_T$  was extended with respect to the default to take muons into account.
- [96] With only selection cuts, the SM backgrounds would be dominated by QCD processes, *cf.* Sec. IV A.
- [97] Beside the term proportional to  $\tan\beta$ , the off diagonal element of the stau mass matrix possesses a term proportional to a softbreaking trilinear coupling. However, unless  $A_0 = \mathcal{O}(1 \text{ TeV})$ , this term plays only a subleading role. We have always set  $A_0 = 0$  in our parameter scans.
- [98] Following Ref. [32] we use the lower stau mass bound from LEP obtained in the  $R$ -parity conserving limit, because LEP did not explore the possibility of a stau LSP decaying via a four-body decay.
- [99] In order to calculate the correct Higgs mass bound we used the respective routine implemented in **SOFTSUSY**.
- [100] This corresponds roughly to an integrated luminosity of  $10 \text{ fb}^{-1}$  at  $\sqrt{s} = 14 \text{ TeV}$ .
- [101] The fit range is crucial and has been determined in an iterated Gaussian fit, which starts with the maximum bin position and the RMS of the histogram and uses the range  $\mu - \sqrt{2 \ln 2} / 2 \cdot \sigma$  to  $200 \text{ GeV}$ , where  $\mu$  is the mean of the previous Gaussian fit and  $\sigma^2$  its variance.
- [102] The efficiencies are nearly identical with and without overlap removal, only the number of fake taus differs significantly as many electrons are also identified as taus in **Delphes**.